

AD-6 261178

2

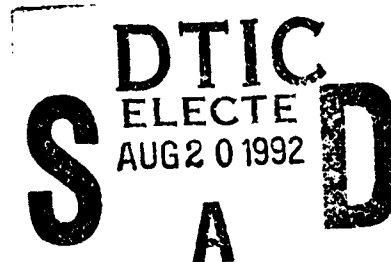
**AD-A256 676**



**PL-TR-92-2124**

# **SCATTERING OF ELASTIC WAVES BY A SPHERICAL INCLUSION**

**Valeri A. Korneev  
Lane R. Johnson**



**Seismographic Station  
University of California  
Berkeley, CA 94720**

**28 April 1992**

**Scientific Report No. 1**

**92-23087**



**APPROVED FOR PUBLIC RELEASE; DISTRIBUTION UNLIMITED**

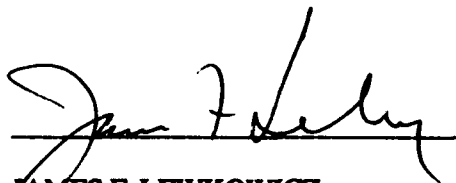


**PHILLIPS LABORATORY  
AIR FORCE SYSTEMS COMMAND  
HANSCom AIR FORCE BASE, MASSACHUSETTS 01731-5000**

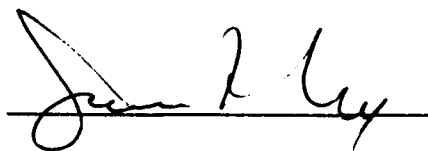
**92 8 19 014**

The views and conclusions contained in this document are those of the authors and should not be interpreted as representing the official policies, either expressed or implied, of the Air Force or the U.S. Government.

This technical report has been reviewed and is approved for publication.



**JAMES F. LEWKOWICZ**  
Contract Manager  
Solid Earth Geophysics Branch  
Earth Sciences Division



**JAMES F. LEWKOWICZ**  
Branch Chief  
Solid Earth Geophysics Branch  
Earth Sciences Division



**DONALD H. ECKHARDT, Director**  
Earth Sciences Division

This document has been reviewed by the ESD Public Affairs Office (PA) and is releasable to the National Technical Information Service (NTIS).

Qualified requestors may obtain additional copies from the Defense Technical Information Center. All others should apply to the National Technical Information Service.

If your address has changed, or if you wish to be removed from the mailing list, or if the addressee is no longer employed by your organization, please notify PL/IMA, Hanscom AFB MA 01731-5000. This will assist us in maintaining a current mailing list.

Do not return copies of this report unless contractual obligations or notices on a specific document requires that it be returned.

REPORT DOCUMENTATION PAGE			Form Approved OMB No. 0704-0188	
Public reporting burden for this collection of information is estimated to average 1 hour per response, including the time for reviewing instructions, searching existing data sources, gathering and maintaining the data needed, and completing and reviewing the collection of information. Send comments regarding this burden estimate or any other aspect of this collection of information, including suggestions for reducing this burden, to Washington Headquarters Services, Directorate for Information Operations and Reports, 1215 Jefferson Davis Highway, Suite 1204, Arlington, VA 22202-4302, and to the Office of Management and Budget, Paperwork Reduction Project (0704-0188), Washington, DC 20503.				
1. AGENCY USE ONLY (Leave blank)		2. REPORT DATE 28 April 1992		3. REPORT TYPE AND DATES COVERED Scientific #1
4. TITLE AND SUBTITLE Scattering of Elastic Waves by a Spherical Inclusion			5. FUNDING NUMBERS PE 62101F PR 7600 TA 09 WU BF  Contract F19628-90-K-0055	
6. AUTHOR(S) Valeri A. Korneev Lane R. Johnson				
7. PERFORMING ORGANIZATION NAME(S) AND ADDRESS(ES) University of California Seismographic Station Berkeley, CA 94720			8. PERFORMING ORGANIZATION REPORT NUMBER	
9. SPONSORING/MONITORING AGENCY NAME(S) AND ADDRESS(ES) Phillips Laboratory Hanscom AFB, MA 01731-5000  Contract Manager: James Lewkowicz/GPEH			10. SPONSORING/MONITORING AGENCY REPORT NUMBER  PL-TR-92-2124	
11. SUPPLEMENTARY NOTES				
12a. DISTRIBUTION/AVAILABILITY STATEMENT  Approved for public release; Distribution unlimited			12b. DISTRIBUTION CODE	
13. ABSTRACT (Maximum 200 words)  A complete and exact solution for the problem of an incident P wave scattered by an elastic spherical inclusion is presented and described. The solution can be obtained from either analytical formulas or stable numerical procedures. A method of estimating the number of terms that must be retained in the harmonic series in order to achieve a specified accuracy is given. The results are investigated by calculating synthetic seismograms, scattering diagrams, and scattering cross sections for a broad frequency band and for both low-velocity and high-velocity inclusions. The fields within the shadow zone are formed primarily from three different types of waves, P waves transmitted through the sphere, P waves diffracted around the sphere, and S waves converted at the boundary of the sphere.  Starting with the exact solution for the scattering of a plane P wave by a homogeneous spherical inclusion, various types of approximate solutions are developed and discussed. The standard Rayleigh and Mie approximations are extended to the case of inclusions having arbitrary contrasts in material properties. For the low contrast case, solutions are developed which are valid over a wide frequency range. Several aspects of these solutions are discussed, including the importance of near-field terms and the relative strength of the scattered P and S fields. The various types of approximate solutions are compared with each other and with the exact solution by calculating and displaying their normalized scattering cross sections.				
14. SUBJECT TERMS Elastic waves Scattering Diffraction			15. NUMBER OF PAGES 76	
			16. PRICE CODE	
17. SECURITY CLASSIFICATION OF REPORT Unclassified	18. SECURITY CLASSIFICATION OF THIS PAGE Unclassified	19. SECURITY CLASSIFICATION OF ABSTRACT Unclassified	20. LIMITATION OF ABSTRACT SAR	

## TABLE OF CONTENTS

Scattering of elastic waves by a spherical inclusion	1
1. Theory and numerical results	
Scattering of elastic waves by a spherical inclusion	41
2. Limitations of asymptotic solutions	

DTIC QUALITY INSPECTED 8

Accession For	
NTIS CRA&I	<input checked="" type="checkbox"/>
DTIC TAB	<input type="checkbox"/>
Unannounced	<input type="checkbox"/>
Justification	
By	
Distribution /	
Availability Codes	
Dist	Avail and/or Special
A-1	

# **Scattering of elastic waves by a spherical inclusion - 1. Theory and numerical results**

*Valeri A. Korneev and Lane R. Johnson*

Department of Geology and Geophysics, University of California,  
and Center for Computational Seismology, Lawrence Berkeley Laboratory,  
Berkeley, California 94720

A complete and exact solution for the problem of an incident P wave scattered by an elastic spherical inclusion is presented and described. The solution can be obtained from either analytical formulas or stable numerical procedures. A method of estimating the number of terms that must be retained in the harmonic series in order to achieve a specified accuracy is given. The results are investigated by calculating synthetic seismograms, scattering diagrams, and scattering cross sections for a broad frequency band and for both low-velocity and high-velocity inclusions. The fields within the shadow zone are formed primarily from three different types of waves, P waves transmitted through the sphere, P waves diffracted around the sphere, and S waves converted at the boundary of the sphere. The relative contribution from these different waves depends upon the distance of the observation point from the sphere.

**Key words:** elastic waves, sphere, scattering, diffraction

## **1. Introduction**

The fact that the earth is not a homogeneous body has forced seismologists to consider scattered waves in their attempts to explain some of the features they observe on seismograms. Elastic wave scattering has been called upon to explain a variety of different phenomena which are routinely observed. These include the phase and amplitude fluctuations of waves arriving at a seismic array (Aki, 1973), the precursors to PKIKP (Haddon and Cleary, 1974), and the codas of local earthquakes (Aki, 1969). In addition, the attenuation of seismic waves is usually interpreted as being a combination of

intrinsic absorption and scattering (Aki, 1980).

The general problem of scattering of elastic waves by a heterogeneity within the earth is a difficult one and analytical solutions are known for only a few special cases, and even in these instances the solutions are complicated and laborious to calculate. Thus, most attempts at interpreting scattered seismic waves have relied upon approximate treatments of the scattering theory. A number of approximations are possible and are related to such parameters as the size of the scatterer, the shape of the scatterer, the distance of the observation point from the scatterer, the magnitude of the heterogeneity, and the number of times the wave has been scattered. Assessing the validity of these approximations is not a simple matter and has been addressed for only some of the approximations (for example, Hudson and Heritage, 1981). The matter is further complicated by the fact that more than one approximation may be involved in the same problem, and it is not always obvious that the different approximations are consistent.

The best method of checking the validity of the approximations which are made in scattering problems is to compare them with exact analytical solutions. In this paper we develop and discuss the properties of one such solution, the scattering of a plane P wave by a spherical inclusion. The method of obtaining the analytical solution is outlined, the numerical methods used in calculating the solution are described, and some of the important features of the solution are described and discussed. The results contained in this paper are the starting point for a companion paper (Korneev and Johnson, 1992), which makes detailed comparisons between various approximations and the exact solution.

In setting up the theoretical problem for elastic wave scattering, one must choose a model which is complicated enough so that it resembles situations found in the earth and at the same time simple enough to allow tractable solutions of the mathematical equations. We have chosen to model a local heterogeneity as a homogeneous elastic sphere surrounded by a homogeneous elastic medium. The elastic constants and density of the spherical inclusion can be arbitrarily different from those of the surrounding medium. The sphere can also be filled with a fluid. The sphere is one of the few objects for which the scattering problem can be solved exactly. It also has the desirable property of being describable by a minimum number of parameters, which makes the interpretation of the analytical and

numerical results relatively simple. Furthermore, scattering by a sphere represents a canonical problem for a more extended class of objects with relatively simple and smooth boundaries, and thus the results presented in this paper contribute to the general understanding of scattering from this class of heterogeneities.

## 2. Theory

The analytical treatment of scattering of elastic waves by a spherical inclusion has a long and rich history, dating back to the classical papers by Clebsch (1863) and Rayleigh (1871). Much of the earlier work was restricted to scalar (acoustic) waves, hollow inclusions, or rigid inclusions. Much of the more recent work on the scattering of elastic waves by a spherical inclusion has been associated with the names of G. I. Petrashen in the USSR and R. Truell in the USA. As early as 1944 Petrashen was studying the scattering problem for an incident P wave, where he made use of a natural spherical vector system which he had developed earlier for the purposes of quantum mechanical problems. The later studies by Petrashen and his students were concerned mostly with obtaining asymptotic representations for different kinds of regular and diffracted waves formed by a sphere (Petrashen, 1946, 1950a, 1950b, 1953; Buldurev and Molotkov, 1958), such as head interference waves for the scalar case (Buldyrev and Molotkov, 1960), failure waves for the scalar case, surface waves on an isolated elastic sphere (Gelchinskij, 1958), and complete solutions for an elastic sphere (Korneev, 1983; Korneev and Petrashen, 1987). Related work includes the theoretical and experimental studies of acoustic waves incident upon an elastic sphere by Nigul et al. (1974). Independently, Truell and his coworkers (Ying and Truell, 1956; Einspruch, Witterholt, and Truell, 1960; Truell, Elbaum, and Chick, 1969) also made important contributions to the solution of this problem. The basic equations that are obtained when displacement potentials are used along with summaries of some of the work mentioned above can be found in such books as Morse and Feshbach (1953) and Pao and Mow (1971).

The basic method followed in the above papers is to write the solutions inside and outside the inclusion in terms of appropriate eigenfunctions of the differential equations and then couple these solutions by matching the boundary conditions on the surface of the inclusion. It is also possible to

formulate this problem as an integral equation by making use of the elastodynamic Green function for a homogeneous medium. Further information on this approach can be found in Miles (1960), Haddon and Cleary (1974), Varatharajulu and Pao (1976), Waterman (1976), Hudson (1977), and Gubernatis et al. (1977a, 1977b).

In this section we outline a method of obtaining the general solution for the scattering of a plane P wave by a spherical inclusion. Although a solution to this problem can be found in several of the papers listed in the previous paragraphs, we repeat it here for completeness and also to introduce a set of spherical basis vectors which are used in our solution but are not common in the English literature. These basis vectors were developed by Petrashen and have properties which are convenient for solving vector function problems with spherical symmetry.

Consider the configuration shown in Figure 1. Joint Cartesian  $\{x,y,z\}$  and spherical  $\{r,\theta,\phi\}$  coordinate systems will be used. Centered about the common origin of these coordinate systems is a sphere of radius  $r = R$ . The volume within this sphere will be denoted by the index  $v = 1$ , while the volume outside will be denoted by  $v = 2$ . The materials inside and outside the sphere will in general be different, and the properties of these materials are completely described by the Lamé parameters and density

$$\lambda_v = \text{const.}, \quad \mu_v = \text{const.}, \quad \rho_v = \text{const.}, \quad (v = 1,2) \quad (2.1)$$

Incident from medium  $v = 2$  is a harmonic disturbance with a displacement field given by

$$\bar{U}_0 = U_0(x,y,z) e^{i\omega t} \quad (2.2)$$

The interaction of this incident wave with the sphere gives rise to additional displacement fields both inside and outside the sphere, and these are denoted by

$$U_v = U_v(x,y,z) e^{i\omega t}, \quad (v = 1,2) \quad (2.3)$$

These additional disturbances will be referred to as the scattered fields. Associated with each field is a stress tensor. We will only need the traction on spherical surfaces and this is given by

$$t_r^{(v)}(U_v) = \lambda_v \nabla \cdot U_v \hat{r} + 2\mu_v \frac{\partial U_v}{\partial r} + \mu_v [\hat{r} \times \nabla \times U_v] \quad (2.4)$$



where  $\hat{\mathbf{r}} = \mathbf{r}/r$  is the unit radius-vector. We also denote the velocities and slownesses of both compressional and shear waves by

$$V_p^{(v)} = \sqrt{\frac{\lambda_v + 2\mu_v}{\rho_v}} \equiv \alpha_v^{-1}, \quad V_s^{(v)} = \sqrt{\frac{\mu_v}{\rho_v}} \equiv \beta_v^{-1} \quad (2.5)$$

The incident field of equation (2.2) and the scattered fields of equation (2.3) must all satisfy the elastodynamic equations of motion in mediums  $v = 1, 2$ ,

$$(\lambda_v + 2\mu_v) \nabla^2 \mathbf{U}_v - \mu_v \nabla \times \nabla \times \mathbf{U}_v + \rho_v \omega^2 \mathbf{U}_v = 0 \quad (2.6)$$

Taken together the fields must satisfy the boundary conditions on the surface of the sphere, which are that the displacement and traction should be continuous. Thus we require that

$$\mathbf{U}_1 = \mathbf{U}_0 + \mathbf{U}_2 \quad \text{and} \quad \mathbf{t}_r^{(1)}[\mathbf{U}_1] = \mathbf{t}_r^{(2)}[\mathbf{U}_0 + \mathbf{U}_2] \quad (2.7)$$

where all of these equations are evaluated at  $r = R$ . We also require that the scattered fields remain finite within the sphere and satisfy a radiation condition at large distances from the sphere

$$\mathbf{U}_2 = \frac{\mathbf{c}(\theta, \phi)}{r} e^{-ikr}, \quad (r \rightarrow \infty) \quad (2.8)$$

where  $k = \omega/V_p^{(2)}$  or  $k = \omega/V_s^{(2)}$ . This is a well-posed problem in that, given the incident wave, the boundary conditions are sufficient to solve for the scattered fields and thus arrive at a unique solution to the problem.

Now let us consider the special case of an incident wave which is a plane harmonic P (compressional) wave propagating in the direction of the positive  $z$  axis. In this case we have

$$\mathbf{U}_0 = e^{-i\omega \alpha_2 z} \hat{\mathbf{z}} \quad (2.9)$$

where  $\hat{\mathbf{z}}$  is a unit vector in the  $z$  direction. We construct the solutions by introducing the system of spherical vectors developed by Petrashen (1945, 1949)

$$\begin{aligned} \mathbf{Y}_{lm}^0 &\equiv \mathbf{Y}_{lm}^0(\theta, \phi) = \mathbf{r} \times \nabla Y_{lm}(\theta, \phi) \\ \mathbf{Y}_{lm}^+ &\equiv \mathbf{Y}_{lm}^+(\theta, \phi) = (l+1) \hat{\mathbf{r}} Y_{lm}(\theta, \phi) - r \nabla Y_{lm}(\theta, \phi) \\ \mathbf{Y}_{lm}^- &\equiv \mathbf{Y}_{lm}^-(\theta, \phi) = l \hat{\mathbf{r}} Y_{lm}(\theta, \phi) + r \nabla Y_{lm}(\theta, \phi) \end{aligned} \quad (2.10)$$

with the usual definitions for the spherical harmonic functions

$$Y_{lm}(\theta, \phi) = e^{im\phi} P_l^m(\cos \theta) \quad , \quad l \geq 0 \quad , \quad (-l \leq m \leq l)$$

This system, whose main features are outlined in Appendix A, leads to particularly simple equations in this problem of spherical symmetry. Using the system of equation (2.10), an arbitrary vector function  $\mathbf{U}$  can be represented in the form

$$\mathbf{U} = \sum_{l \geq 0, |m| \leq l} \left\{ \psi_{lm}^0(r) \mathbf{Y}_{lm}^0 + \psi_{lm}^+(r) \mathbf{Y}_{lm}^+ + \psi_{lm}^-(r) \mathbf{Y}_{lm}^- \right\} \quad (2.11)$$

where the  $\psi_{lm}(r)$  are unspecified radial functions at this point.

The particular incident wave of equation (2.9) has the representation

$$\mathbf{U}_0 = \sum_{l \geq 0} \left\{ j_{l+1}(\omega \alpha_2 r) \mathbf{Y}_{l0}^+ - j_{l-1}(\omega \alpha_2 r) \mathbf{Y}_{l0}^- \right\} e^{-i\frac{\pi}{2}(l+1)} \quad (2.12)$$

where the  $j_k(x)$  are spherical Bessel functions. The displacement fields of the scattered waves  $\mathbf{U}_1$  and  $\mathbf{U}_2$  from equation (2.3) could also be represented in terms of a series of the spherical vectors of equation (2.10). Making use of the structure of the series in equation (2.12) for the incident wave and the orthogonal properties of the spherical vectors (see Appendix A), it is possible to show that  $\mathbf{U}_1$  and  $\mathbf{U}_2$  can be represented by

$$\mathbf{U}_1 = \sum_{l \geq 0} \left\{ \left[ a_l^{(1)} j_{l+1}(\omega \alpha_1 r) + l b_l^{(1)} j_{l+1}(\omega \beta_1 r) \right] \mathbf{Y}_{l0}^+ + \left[ -a_l^{(1)} j_{l-1}(\omega \alpha_1 r) + (l+1) b_l^{(1)} j_{l-1}(\omega \beta_1 r) \right] \mathbf{Y}_{l0}^- \right\} e^{-i\frac{\pi}{2}(l+1)} \quad (2.13)$$

$$\mathbf{U}_2 = \sum_{l \geq 0} \left\{ \left[ a_l^{(2)} h_{l+1}(\omega \alpha_2 r) + l b_l^{(2)} h_{l+1}(\omega \beta_2 r) \right] \mathbf{Y}_{l0}^+ + \left[ -a_l^{(2)} h_{l-1}(\omega \alpha_2 r) + (l+1) b_l^{(2)} h_{l-1}(\omega \beta_2 r) \right] \mathbf{Y}_{l0}^- \right\} e^{-i\frac{\pi}{2}(l+1)} \quad (2.14)$$

where  $a_l^{(v)}$  and  $b_l^{(v)}$  are now unknown scalars and the  $h_k(x)$  are spherical Hankel functions of the second kind. Note that the spherical Bessel functions  $j_k(x)$  of equation (2.13) are finite throughout the inclusion and the spherical Hankel functions  $h_k(x)$  of equation (2.14) have asymptotic representations for large argument that satisfy the condition in equation (2.8). Also note that with the basis vectors being used here, the displacements in equations (2.13) and (2.14) separate into compressional and shear fields, so that either equation can be put in the form

$$\mathbf{U}_v = \mathbf{U}_v^p + \mathbf{U}_v^s \quad (2.15)$$

with the  $a_l^{(v)}$  associated with the P field  $\mathbf{U}_v^p$  and the  $b_l^{(v)}$  associated with the S field  $\mathbf{U}_v^s$ , and with the following conditions satisfied

$$\nabla \times \mathbf{U}_v^p \equiv 0, \quad \nabla \cdot \mathbf{U}_v^s \equiv 0. \quad (2.16)$$

To determinate the coefficients  $a_l^{(v)}$  and  $b_l^{(v)}$  in equations (2.13) and (2.14) we have to satisfy the boundary conditions of equation (2.7). Making the necessary substitutions, evaluating the expressions for  $r = R$ , and using the orthogonal properties of the spherical vectors, one arrives at a separate set of linear equations for each value of  $l$ . When  $l = 0$  one can take advantage of the fact that  $\mathbf{Y}_{00}^- = 0$  to get the abbreviated set of equations

$$W_0 \begin{bmatrix} a_0^{(1)} \\ a_0^{(2)} \end{bmatrix} = \begin{bmatrix} j_1(\xi_2) \\ O_2 \end{bmatrix} \quad (2.17)$$

where

$$W_0 = \begin{bmatrix} j_1(\xi_1) & -h_1(\xi_2) \\ \kappa O_1 & -\bar{O}_2 \end{bmatrix} \quad (2.18)$$

$$O_v = \frac{\gamma_v}{\xi_v} \left[ \frac{\xi_v}{\gamma_v^2} j_0(\xi_v) - 4j_1(\xi_v) \right]$$

$$\bar{O}_2 = \frac{\gamma_2}{\xi_2} \left[ \frac{\xi_2}{\gamma_2^2} h_0(\xi_2) - 4h_1(\xi_2) \right]$$

$$\begin{aligned} \xi_v &= \alpha_v \omega R & \eta_v &= \beta_v \omega R \\ \gamma_v &= \frac{\alpha_v}{\beta_v} & \kappa &= \frac{\rho_1 \beta_2}{\rho_2 \beta_1} \end{aligned} \quad (2.19)$$

When  $l \geq 1$  a full set of four equations with four unknowns is obtained of the form

$$W_l F_l = \bar{F}_l \quad (2.20)$$

where  $F_l$  and  $\bar{F}_l$  are the column matrices

$$F_l = \left[ a_l^{(1)}, b_l^{(1)}, a_l^{(2)}, b_l^{(2)} \right]^T \quad (2.21)$$

and

$$\bar{F}_l = \left[ j_{l+1}(\xi_2), -j_{l-1}(\xi_2), C_2^+, C_2^- \right]^T \quad (2.22)$$

and the matrix  $W_l$  is given by

$$W_l = \begin{bmatrix} j_{l+1}(\xi_1) & l j_{l+1}(\eta_1) & -h_{l+1}(\xi_2) & -l h_{l+1}(\eta_2) \\ -j_{l-1}(\xi_1) & (l+1) j_{l-1}(\eta_1) & h_{l-1}(\xi_2) & -(l+1) h_{l-1}(\eta_2) \\ \kappa C_1^+ & \kappa l D_1^+ & -\bar{C}_2^+ & -l \bar{D}_2^+ \\ \kappa C_1^- & -\kappa(l+1) D_1^- & -\bar{C}_2^- & (l+1) \bar{D}_2^- \end{bmatrix} \quad (2.23)$$

The following notations are used here

$$\left. \begin{matrix} C_v^+ \\ C_v^- \end{matrix} \right\} = \frac{\gamma_v}{\xi_v} \left[ \frac{\xi_v}{\gamma_v^2} j_l(\xi_v) - 2 \left\{ \begin{matrix} (l+2) j_{l+1}(\xi_v) \\ (l-1) j_{l-1}(\xi_v) \end{matrix} \right\} \right]$$

$$\left. \begin{matrix} \bar{C}_v^+ \\ \bar{C}_v^- \end{matrix} \right\} = \frac{\gamma_v}{\xi_v} \left[ \frac{\xi_v}{\gamma_v^2} h_l(\xi_v) - 2 \left\{ \begin{matrix} (l+2) h_{l+1}(\xi_v) \\ (l-1) h_{l-1}(\xi_v) \end{matrix} \right\} \right]$$

$$\left. \begin{matrix} D_v^+ \\ D_v^- \end{matrix} \right\} = \frac{1}{\eta_v} \left[ \eta_v j_l(\eta_v) - 2 \left\{ \begin{matrix} (l+2) j_{l+1}(\eta_v) \\ (l-1) j_{l-1}(\eta_v) \end{matrix} \right\} \right]$$

$$\left. \begin{matrix} \bar{D}_v^+ \\ \bar{D}_v^- \end{matrix} \right\} = \frac{1}{\eta_v} \left[ \eta_v h_l(\eta_v) - 2 \left\{ \begin{matrix} (l+2) h_{l+1}(\eta_v) \\ (l-1) h_{l-1}(\eta_v) \end{matrix} \right\} \right]$$

It can be shown that the determinants of equations (2.18) and (2.23) are always different from zero, so in principle it is always possible to solve the systems of equations (2.17) and (2.20) for the unknown coefficients  $a_l^{(v)}$  and  $b_l^{(v)}$  for any  $l$ . However, because of the asymptotic properties of the

matrix elements, numerical difficulties can be encountered when solving these systems of equations. This will be discussed in the next section.

Finally, note that the coefficients  $a_l^{(v)}$  and  $b_l^{(v)}$  for any  $l$  are completely defined by the member of the series in equation (2.12) for the incident wave with the same  $l$ . That is, there is no coupling between harmonics associated with different values of  $l$ . This means that a scattering problem for the sphere with an incident wave represented by any member of equation (2.12) with index  $l$  could be considered, and the results would be the corresponding members of equations (2.17) and (2.20) with the same index  $l$ . To illustrate this point we will show how the solution for an incident wave generated by a point pressure source can be obtained by a slight modification of the solution for a plane wave source developed above. Consider a point pressure source located at the point  $\mathbf{R}_0 = (Z_0, 0, 0)$  where  $Z_0 > R$ . This will generate a displacement field  $\mathbf{U}_0$  of a spherical P-wave

$$\mathbf{U}_0 = -\nabla \frac{e^{-ik_p |\mathbf{r}-\mathbf{R}_0|}}{|\mathbf{r}-\mathbf{R}_0|} = -ik_p^2 \sum_{l \geq 0} \left\{ j_{l+1}(k_p r) \mathbf{Y}_{l0}^+ - j_{l-1}(k_p r) \mathbf{Y}_{l0}^- \right\} h_l(k_p Z_0) \quad (2.24)$$

Each member of the series in equation (2.24) differs from that in equation (2.12) by the coefficient

$$c_l = -ik_p^2 e^{i\frac{\pi}{2}(l+1)} h_l(k_p Z_0)$$

Thus the solution for the point pressure source is simply obtained by multiplying the members of equations (2.13) and (2.14) by  $c_l$ . The equations (2.17) and (2.20) are unchanged.

### 3. Numerical considerations

To calculate the scattered fields  $\mathbf{U}_1$  and  $\mathbf{U}_2$  using the series in equations (2.13) and (2.14) we have to solve the linear systems of equations (2.17) and (2.20) for all  $l \geq 0$ . These systems of equations are generally solved by numerical methods, which means that the numerical stability of the calculations are a concern. The coefficients of the matrices  $\mathbf{W}_l$  in these systems include spherical Bessel and Hankel functions, whose features for  $l \gg 1$  are characterized by the formulas

$$j_l(z) \approx \frac{1}{z} \cos \left[ z - \frac{\pi}{2}(l+1) \right], \quad h_l(z) \approx \frac{1}{z} e^{-i(z - \frac{\pi}{2}(l+1))} \quad (3.1)$$

if  $z \gg l$ , and

$$j_l(z) \approx \frac{1}{2z\sqrt{y}} \left( \frac{2y}{e} \right)^{-(l+\frac{1}{2})}, \quad h_l(z) \approx \frac{i}{z\sqrt{y}} \left( \frac{2y}{e} \right)^{l+\frac{1}{2}} \quad (3.2)$$

if  $z \ll l$ , where

$$y = \frac{l + \frac{1}{2}}{z}$$

Because of different ratios between  $l$  and the arguments  $\xi_1$ ,  $\xi_2$ ,  $\eta_1$ , and  $\eta_2$  of the functions  $j_l$  and  $h_l$  that appear in equation (2.23), the orders of the different columns of this matrix can become quite different. In particular, for the case  $l \rightarrow \infty$  the coefficients in the two first columns go to zero while the other coefficients go to infinity. In such a situation numerical calculations on a computer can become unstable before achieving the necessary accuracy.

To avoid this situation, we redefine the unknown variables  $a_l^{(v)}$ ,  $b_l^{(v)}$  as new ones  $x_l^{(v)}$ ,  $y_l^{(v)}$  by the formulas

$$\begin{aligned} a_l^{(1)} &= h_l(\xi_1) x_1^{(1)}, & b_l^{(1)} &= h_l(\eta_1) y_1^{(1)} \\ a_l^{(2)} &= h_l^{-1}(\xi_2) x_1^{(2)}, & b_l^{(2)} &= h_l^{-1}(\eta_2) y_1^{(2)} \end{aligned} \quad (3.3)$$

Now, if we let the unknown column matrix be

$$X_l = \left[ x_l^{(1)}, y_l^{(1)}, x_l^{(2)}, y_l^{(2)} \right]^T \quad (3.4)$$

the system of equation (2.20) will be

$$\bar{W}_l X_l = \bar{F}_l \quad (3.5)$$

where the column matrix  $\bar{F}_l$  is the same as in equation (2.22), and  $\bar{W}_l$  can be obtained from equation (2.23) by multiplying its columns by  $h_l(\xi_1)$ ,  $h_l(\eta_1)$ ,  $h_l^{-1}(\xi_2)$ ,  $h_l^{-1}(\eta_2)$ , respectively. Now the coefficients of the matrix  $\bar{W}_l$  have values of approximately the same order (they differ from each other no more than by a coefficient of order  $l$ ) and the numerical difficulty mentioned above vanishes.

The change in variable given by equation (3.3) is also helpful in solving another numerical problem, that of determining how much of the infinite series of the solutions in equations (2.13) and (2.14)

must be retained in order to achieve a given accuracy. Note that the unknown coefficients now are of the same order as the members of  $\tilde{F}_l$

$$x_l^{(v)} \sim y_l^{(v)} \sim j_l(\xi_2) \quad (3.6a)$$

and for  $l > \xi_2$  we obtain the estimate

$$x_{l_0}^{(v)} \sim y_{l_0}^{(v)} \sim \frac{1}{2\sqrt{\xi_2 l_0}} \left[ 1 - \frac{N + \frac{1}{2}}{l_0 + \frac{1}{2}} \right]^{l_0 + \frac{1}{2}} \approx \frac{1}{2\sqrt{\xi_2 l_0}} e^{-N} \quad (3.6b)$$

where

$$l_0 = \frac{e \xi_2}{2} + N, \quad (N > 1) \quad (3.7)$$

is taken to be sufficiently large ( $l_0 \gg 1$ ). Thus, the coefficients  $x_l^{(v)}$  and  $y_l^{(v)}$  go to zero exponentially

when  $l \geq \frac{e \xi_2}{2} + N$  and  $N \rightarrow \infty$ . Using the following relations obtained from equation (3.3)

$$\left. \begin{aligned} a_l^{(1)} j_{l \pm 1}(\omega \alpha_1 r) &= x_l^{(1)} h_l(\xi_1) j_{l \pm 1}(\xi_1 \frac{r}{R}) \\ b_l^{(1)} j_{l \pm 1}(\omega \beta_1 r) &= y_l^{(1)} h_l(\eta_1) j_{l \pm 1}(\eta_1 \frac{r}{R}) \end{aligned} \right\} \quad (r < R)$$

$$\left. \begin{aligned} a_l^{(2)} h_{l \pm 1}(\omega \alpha_2 r) &= x_l^{(2)} h_{l \pm 1}(\xi_2 \frac{r}{R}) / h_l(\xi_2) \\ b_l^{(2)} h_{l \pm 1}(\omega \beta_2 r) &= y_l^{(2)} h_{l \pm 1}(\eta_2 \frac{r}{R}) / h_l(\eta_2) \end{aligned} \right\} \quad (r > R)$$

and the "limited" character of the values

$$\left| h_{l \pm 1}(\xi \frac{r}{R}) / h_l(\xi) \right|, \quad \left| h_l(\xi) j_{l \pm 1}(\xi \frac{r}{R}) \right|$$

it is clear that the series in equations (2.13) and (2.14) converge at a rate that is equal to or greater than the series in equation (2.12). Therefore, if we take the first  $l_0$  members of the series, with  $l_0$  specified by equation (3.7), the absolute error of the calculations will not be greater than a value of order  $e^{-N}$ .

When any of the arguments  $\xi_v$ ,  $\eta_v$  is no more than  $\xi_2$ , the error in the respective series decreases with increasing  $r$  as  $(r/R)^{l_0}$  in medium  $v = 1$  ( $r < R$ ) and as  $(R/r)^{l_0}$  in medium  $v = 2$  ( $r > R$ ). Thus, given a error tolerance for the calculations of the fields  $U_v(r, \theta)$ , we can estimate a number  $l_0$  for any

frequency  $\omega$  and sum the series in equations (2.13) and (2.14) for  $l \leq l_0$ . Test calculations showed that  $N = 15$  in equation (3.7) is sufficient to give an accuracy of  $10^{-8}$  or better.

As mentioned at the beginning of this section, the system of equations (2.20), or equivalently (3.5), are generally solved by numerical methods. However, analytical solutions of these systems are possible, although laborious, requiring the equivalent of inverting a matrix of rank four. This has been done and the results are given in Appendix B. Having two different solutions of the same basic equations is quite useful in checking the stability and accuracy of both solutions. Thus the analytical solutions of Appendix B were used to check the solutions that were obtained by numerically solving equation (3.5). This comparison showed that for  $l_0$  given by equation (3.7) with  $N = 15$  the numerical solution of equation (3.5) is stable and gives the same result as the analytical solutions. For  $N > 15$  (accuracies better than  $10^{-8}$ ) the calculations revealed that the analytical solution gave more accurate results. It should be mentioned here that all of the calculations discussed in this paper were done with double precision arithmetic.

There is another way of estimating the accuracy of the calculations without considering the properties of the coefficients  $a_l$  and  $b_l$ . This approach takes advantage of the observation made earlier that there is no coupling between harmonics associated with different values of  $l$ . Thus one considers the expression for the incident wave in equation (2.12) evaluated on the surface of the sphere ( $r = R$ ) and truncates the series at a value of  $l$  that gives the desired accuracy in representing the incident wave. Then the  $a_l$  and  $b_l$  summed up to this same value of  $l$  can be considered as either the exact solution to the truncated version of the incident wave or as the approximate solution to the analytical version of the incident wave having the desired accuracy.

#### 4. Scattering cross sections

A useful method of characterizing scattering by an object is to calculate the energy of the scattered waves and compare it to the energy of the incident wave. Various forms of this ratio between the scattered and incident energies are called scattering cross sections. The energy of the scattered waves can be obtained by calculating the energy flux of scattered waves through a surface  $S$  that completely



surrounds the object. Noting that the energy flux per unit time through a surface element  $ds$  having a normal  $\mathbf{n}$  is given by  $(\dot{\mathbf{U}} \cdot \mathbf{t}_n[\mathbf{U}])$  and that the energy flux averaged over one period is  $\omega \text{Im}(\mathbf{U} \cdot \mathbf{t}_n^*[\mathbf{U}])/2$ , then the total energy flux per period through the surface  $S$  is given by

$$F = \frac{\omega}{2} \text{Im} \int_S (\mathbf{U} \cdot \mathbf{t}_n^*[\mathbf{U}]) ds \quad (4.1)$$

where (\*) means the complex conjugate. The same reasoning applied to the incident P wave yields an energy flux per unit area of the wave front of  $\omega^2 \alpha_2 (\lambda_2 + 2\mu_2)/2$ .

Now we follow Truell et al. (1969) and define a normalized cross section as the ratio of the flow of total energy carried outward by the scattered waves to the rate of flow in the incident wave through a normal area equal to the cross-sectional area of the object (geometric shadow of the object). In our case we let  $S$  be a spherical surface of radius  $r_0$  with  $r_0 > R$  and the normalized cross section is given by

$$\sigma_N = \text{Im} \int_{r=r_0} \frac{\Phi ds}{\omega \alpha_2 (\lambda_2 + 2\mu_2) \pi R^2}$$

where  $\Phi$  can be calculated by using either of the formulas

$$\Phi = (\mathbf{U}_2 \cdot \mathbf{t}_r^*[\mathbf{U}_2]) \quad (4.2a)$$

or

$$\Phi = -(\mathbf{U}_2 \cdot \mathbf{t}_r^*[\mathbf{U}_0]) - (\mathbf{U}_0 \cdot \mathbf{t}_r^*[\mathbf{U}_2]) \quad (4.2b)$$

The second expression for  $\Phi$  is easily obtained from the fact that the scatterer generates no additional energy, which leads to the conditions that for both the incident wave  $\mathbf{U}_0$  and the total field  $\mathbf{U}_0 + \mathbf{U}_2$  there is zero net energy flux across the surface  $S$  so long as it is entirely contained in medium  $v=2$ .

Using equation (2.4) for the traction vector, the series in equations (2.11) and (2.14) for  $\mathbf{U}_0$  and  $\mathbf{U}_2$ , and orthogonal properties of the spherical vectors, we can obtain two different expressions for  $\sigma_N$

$$\sigma_N = 4 \sum_{l \geq 0} (2l+1) \left\{ \left| \frac{a_l^{(2)}}{\xi_2} \right|^2 + l(l+1) \gamma_2 \left| \frac{b_l^{(2)}}{\eta_2} \right|^2 \right\} \quad (4.3a)$$

or

$$\sigma_N = -4 \sum_{l \geq 0} (2l+1) \frac{\operatorname{Re} a_l^{(2)}}{\xi_2^2} \quad (4.3b)$$

This result together with the earlier noted fact that the coefficients for different values of  $l$  are not coupled means that we must have

$$\left| a_l^{(2)} \right|^2 + l(l+1) \gamma_2^3 \left| b_l^{(2)} \right|^2 = -\operatorname{Re} a_l^{(2)} \quad (4.4)$$

for any value of  $l$ . This relationship is useful in verifying numerical calculations.

The function  $\sigma_N$  from equation (4.3) is closely connected with the value of the field  $U_2(r, \theta)$  of scattered waves that is observed along the positive  $z$  axis for large  $r$  ( $r \gg 2\pi V_p/\omega$ ). Using asymptotic expressions for the spherical Hankel functions in equation (2.14) we obtain

$$\begin{aligned} U_2(r, 0) &= i \hat{z} \frac{e^{-i\xi_2 r}}{\xi_2 r} R \sum_{l \geq 0} (2l+1) a_l^{(2)} \left[ 1 + O\left(\frac{1}{r}\right) \right] \\ &= \hat{z} \frac{e^{-i\xi_2 r}}{r} A_0 \left[ 1 + O\left(\frac{1}{r}\right) \right] \end{aligned} \quad (4.5)$$

where

$$A_0 = i \frac{R}{\xi_2} \sum_{l \geq 0} (2l+1) a_l^{(2)}$$

Comparing equation (4.5) with (4.3b) we have

$$\sigma_N = -4 \frac{\operatorname{Im} A_0}{R \xi_2} \quad (4.6)$$

which is analogous to an optical theorem for elastodynamics. This expression in equation (4.6) is a useful relationship between the amplitude of the forward-scattered field and the total energy scattered in all directions by the obstacle.

## 5. Numerical results

One of the primary purposes of this investigation was to gain an understanding of the features of waves scattered by a local spherical heterogeneity. This problem can be studied with approximate methods, such as ray theory, but it is not always clear if the information provided about amplitudes and waveforms is accurate. With the results presented earlier in this paper, it is possible to calculate these scattered waves with the assurance that the results are complete and accurate. Unfortunately, the results such as equations (2.13) and (2.14) are not very revealing in the form of an analytical series and must first be converted to some graphical form, such as synthetic seismograms or scattering cross sections, before the physical properties of the scattered waves become apparent.

We are interested in knowing what types of waves are scattered by a sphere and particularly interested in understanding where the scattered waves with the largest amplitudes can be found in the region surrounding the sphere. It is possible to argue that the main features of such waves that are scattered by a sphere will be approximately the same for a wide class of smoothly-shaped three-dimensional heterogeneities, and this broadens the utility of the results presented in this paper for providing insight into realistic seismological problems.

First consider the matter of what types of waves are scattered by the sphere and their relative amplitudes. These effects are best observed in the time domain, which requires that the frequency domain solutions obtained in this paper be transformed to the time domain. This was done by applying a numerical Fourier transform to the solutions and by assuming a broad band pulse as the form of the input wave. This source pulse had constant amplitudes in the frequency band between 0.00 and 64.0 Hz with a sampling interval of 0.25 Hz, which means that the pulse contained wavelengths that ranged from more than one order of magnitude smaller than the radius of the sphere to more than an order of magnitude larger. Synthetic seismograms were calculated for the positions that are shown in Figure 1, which lie on a line offset a distance  $z$  from the center of the sphere in the direction of forward scattering and extending from the center of the shadow into the fully illuminated zone. Because of the symmetry of the problem, there are only two non-zero components to the solutions,  $U_x = U_x(x, 0, z, t)$  and  $U_z = U_z(x, 0, z, t)$ .

The solutions presented in this paper can be calculated for arbitrary elastic properties inside and outside the sphere, including the case of a fluid inside the sphere. Here we present results for two models, one representing a low-velocity scatterer and the other representing a high-velocity scatterer.

The elastic parameters for these two models are as follows:

$$\begin{aligned}
 \text{model 1} \quad - \quad & V_p^{(1)} = 4.5 \text{ km/s} , \quad V_s^{(1)} = 2.6 \text{ km/s} , \quad \rho_1 = 2.3 \text{ gm/cm}^3 \\
 & V_p^{(2)} = 6.0 \text{ km/s} , \quad V_s^{(2)} = 3.5 \text{ km/s} , \quad \rho_2 = 2.7 \text{ gm/cm}^3 \\
 \text{model 2} \quad - \quad & V_p^{(1)} = 7.5 \text{ km/s} , \quad V_s^{(1)} = 4.4 \text{ km/s} , \quad \rho_1 = 3.1 \text{ gm/cm}^3 \\
 & V_p^{(2)} = 6.0 \text{ km/s} , \quad V_s^{(2)} = 3.5 \text{ km/s} , \quad \rho_2 = 2.7 \text{ gm/cm}^3
 \end{aligned}$$

Note that there is only one physical dimension in this problem, the radius of the sphere  $R$ . Thus all of the other parameters in the problem can be scaled with respect to this parameter, which is given a value of unity in the results that follow. The velocities and frequencies scale with  $R$  in the sense that the results are invariant so long as the expressions of equation (2.19) and the ratio  $r/R$  remain constant.

Synthetic seismograms are shown for three different values of the offset distance from the sphere  $z$  in Figures 2, 3, and 4. The results for the low velocity scatterer (model 1) are shown in the upper parts of these figures and those for a high velocity scatterer (model 2) are shown in the lower parts. In all of these figures a distance of 1 km along the  $x$  axis represents the edge of the geometrical shadow, since the value  $R = 1 \text{ km}$  was used for the radius of the sphere.

It is useful to associate geometrical ray paths with the primary features of the synthetic seismograms. Within the forward shadow there are three main types of scattered waves. These are:

1) A compressional refracted wave  $P_2P_1P_2$  that goes through the sphere. 2) A shear refracted wave that goes through the sphere as  $P_2P_1S_2$  for a low-velocity sphere and as  $P_2S_1S_2$  for a high-velocity sphere. 3) A compressional diffracted wave  $P_2\hat{P}_2P_2$  that goes around the surface of the sphere. The relative contributions of these different waves to the total seismogram depends upon the offset distance  $z$  from the center of the sphere.

For near offset distances  $z = 2R$  (Figure 2), the wave  $P_2P_1P_2$  dominates the first arrivals within the shadow on the  $z$  component. For a low velocity sphere (model 1) it has a reversed polarity and

arrives after the wave diffracted around the outside of the sphere. Note that there is a strong focusing along the axis for the low-velocity sphere but not the high-velocity sphere. The diffracted wave  $P_2\hat{P}_2P_2$  has a smaller amplitude within the deep shadow at this offset distance. This low-frequency wave loses amplitude exponentially along its ray path around the sphere and is delayed in time with respect to the undisturbed incident wave. The shear waves  $P_2P_1S_2$  (low-velocity case) and  $P_2S_1S_2$  (high-velocity case) are strong on the  $x$  component and have a compound wave structure, involving a caustic and two diffracted waves. The caustic is due to the fact that the sphere is a low-velocity zone for both of these waves, and extending beyond this caustic are low-frequency diffracted waves that attenuate rapidly with distance. For the low-velocity sphere this diffraction from the caustic begins to interfere with the  $P_2P_1P_2$  wave at this offset distance. Behind this caustic and its diffraction is the wave that has been refracted through the opposite side of the sphere and thus arrives at a later time. Along this branch of the wave there is a transition from a geometrical ray arrival to a diffracted wave that continues on to greater distances, although the point of this transition is not obvious on the seismograms. Note that, because of focusing effects and near field terms that are important at this offset distance, these waves have significant amplitudes on the  $z$  component of motion near the center of the shadow. In fact, at  $x = 0$ , we have the unusual situation of an  $S$  wave that appears only on the  $z$  component.

For medium offset distances  $z = 4R$  (Figure 3), all three of the waves  $P_2P_1P_2$ ,  $P_2\hat{P}_2P_2$ , and  $P_2S_1S_2$  have comparable amplitudes. The waves  $P_2P_1P_2$  and  $P_2\hat{P}_2P_2$  arrive closely in time and interfere with each other. The  $P_2P_1S_2$  and  $P_2S_1S_2$  waves are now separated in time from the other phases and their compound nature is clearly evident.

For the larger offset distances  $z = 8R$  (Figure 4), the wave  $P_2\hat{P}_2P_2$  is dominant on the  $z$  components, as the shadow is not nearly so deep as at the smaller offset distances. The wave  $P_2P_1P_2$  which has passed through the sphere is relatively small compared to the wave which has diffracted around it. On the  $x$  components the waves  $P_2P_1S_2$  and  $P_2S_1S_2$  are the dominant arrivals and still display their compound wave forms. It is worth commenting on the reason why the  $P_2P_1S_2$  wave is the dominant shear wave arrival for the low-velocity case, while  $P_2S_1S_2$  is dominant for the high-

velocity case. These are the S waves that see the smallest change in material properties upon both entering and leaving the sphere, and thus the amount of energy lost to reflection and also the amount of strong focusing is minimized. In contrast, the wave  $P_2S_1S_2$  for the low-velocity case encounters a large change in velocity upon entering the sphere, which leads to more energy lost to reflected waves and also causes focusing so strong that the focal point lies within the sphere. Likewise, the wave  $P_2P_1S_2$  for the high-velocity case encounters a large change in velocity upon leaving the sphere.

It should be emphasized that, regardless of the distance from the scatterer, there is a significant amount of motion on the  $x$  component. Recall that the displacement on this component would be zero if the sphere were not present, so we see that scattering is an effective means of transferring motion from one component of motion to an orthogonal component in the direction of forward propagation. At the larger offset distances and for both the low-velocity case and the high-velocity case the shear waves are the dominant contributor to the  $x$  - component seismograms.

A slightly different presentation of some of the data from Figures 2, 3, and 4 is shown in Figure 5. Here the seismograms for the  $z$  component at the center of the shadow are shown as a function of the offset distance  $z$ . They show quite clearly how the dominant wave type in the shadow changes from  $P_2P_1P_2$  at small  $z$  to  $P_2\hat{P}_2P_2$  at large  $z$  for the cases of both the low velocity inclusion and the high velocity inclusion. Note that for the low velocity inclusion the  $P_2\hat{P}_2P_2$  wave is the first arrival, whereas for the high velocity sphere it is the  $P_2P_1P_2$  wave that arrives first. This figure also illustrates how the low velocity sphere is much more effective in focusing energy into the shadow than is the high velocity sphere.

These results show that, depending upon the distance of the observation point from the scattering object, the dominant part of the seismic field in the shadow zone may be composed of waves having a fundamentally different nature. Moreover, in the case of low frequencies it may be difficult to separate these different waves from each other on the basis of travel times. It would appear that results of this type would be applicable to various types of seismic tomographic methods. For instance, the results in Figure 5 show quite clearly that at observation points distant from the inclusion more than a few times its dimension, the dominant wave has been diffracted around the obstacle rather than passing through it,

which differs from the common assumption made in seismic transmission tomography. Because of this, the travel time anomaly will decrease with distance from the inclusion. Obviously, when solving inverse problems to obtain estimates of the properties of the scattering object, it is important to have a proper understanding of what types of waves are dominating the seismograms in order that the correct algorithms can be applied.

So far we have considered only forward scattered waves and the results have been illustrated with broad band time domain seismograms. To obtain a better understanding of how the scattered fields depend upon frequency and also to expand the spatial coverage to include back scattered waves, it is convenient to consider scattering diagrams. The field  $U_2$  from equation (2.14) can be represented in the form

$$U_2 = \left[ U_p(\theta) \right]_r \hat{r} + \left[ U_p(\theta) \right]_\theta \hat{\theta} + \left[ U_s(\theta) \right]_r \hat{r} + \left[ U_s(\theta) \right]_\theta \hat{\theta} \quad (5.1)$$

Then, using equation (2.14) and the definitions of the spherical vectors, we obtain the following expressions for the scattering diagrams for the P and S fields

$$\begin{aligned} \left[ U_p(\theta) \right]_r &= - \sum_{l \geq 0} a_l^{(2)} (2l+1) e^{-i\frac{\pi}{2}(l+1)} \frac{\partial h_l(\xi)}{\partial \xi} P_l(\cos \theta) \\ \left[ U_p(\theta) \right]_\theta &= - \sum_{l \geq 0} a_l^{(2)} (2l+1) e^{-i\frac{\pi}{2}(l+1)} \frac{h_l(\xi)}{\xi} \frac{\partial P_l(\cos \theta)}{\partial \theta} \\ \left[ U_s(\theta) \right]_r &= \sum_{l \geq 1} b_l^{(2)} l(l+1)(2l+1) e^{-i\frac{\pi}{2}(l+1)} \frac{h_l(\eta)}{\eta} P_l(\cos \theta) \\ \left[ U_s(\theta) \right]_\theta &= \sum_{l \geq 1} b_l^{(2)} (2l+1) e^{-i\frac{\pi}{2}(l+1)} \left[ \frac{\partial h_l(\eta)}{\partial \eta} + \frac{h_l(\eta)}{\eta} \right] \frac{\partial P_l(\cos \theta)}{\partial \theta} \end{aligned} \quad (5.2)$$

where we have assumed that the parameters

$$\xi = \frac{\omega r}{V_p^{(2)}} \quad , \quad \eta = \frac{\omega r}{V_s^{(2)}} \quad (5.3)$$

are evaluated for any  $r > R$ .

Scattering diagrams for six different ratios of  $R/\lambda$  that range from less than 0.1 to greater than 3.0 and for both models are shown in Figure 6, where the radius of the observation point  $r$  is taken large enough that near-field terms are small and the scattered P and S waves have their natural polarizations. A number of interesting results emerge from the study of these figures. First, at low frequencies more of the incident P field is converted to scattered S fields than to scattered P fields, while at high frequencies just the opposite occurs. Second, at low frequencies the portions of the incident field which are forward scattered and back scattered are comparable, whereas at high frequencies most of the scattered field lies in the forward direction. At the highest frequencies we approach the case of only generating a forward scattered P field. Third, in terms of the shapes and amplitudes of the scattering diagrams, there are only minor differences between the case of the low velocity inclusion and that of the high velocity inclusion. This is consistent with the results shown in Figures 2-5, where the differences between the low and high velocity case are most pronounced at small distances from the inclusion and tend to diminish at larger distances. Obviously, the near field parts of the solution are more sensitive to the sign of the velocity anomaly of the inclusion than are the far field parts.

Finally, to obtain even more detailed information about the frequency dependence of the scattered fields, it is instructive to consider the scattering cross sections defined in Section 4. These scattering cross sections are plotted for both the low velocity inclusion and the high velocity inclusion in Figure 7. An interesting result shown here is that at low frequencies ( $k_p R < 2$ ) more energy is scattered into the S field than into the P field, with the ratio reaching a factor of 2 or more in some ranges. At high frequencies ( $k_p R$  greater than about 5), the scattered energy flux is primarily in the P field. In this range the long large amplitude oscillations are caused by interference between  $P_2 P_1 P_2$  and  $P_2 \hat{P}_2 P_2$  waves. The short small amplitude oscillations that appear only for the case of the low velocity sphere are caused by the focusing characteristic of a low-velocity inhomogeneity, essentially the waves multiply reflected within the sphere that are evident in Figure 5.

In both the scattering diagrams of Figure 6 and the scattering cross sections of Figure 7 the amplitudes of the scattered fields have been displayed, but information about their phases are not shown. It is important to remember that outside the sphere the total solution consists of the sum of the



incident field  $U_0$  and the scattered field  $U_2$ , and these two fields can add either constructively or destructively. From a physical viewpoint it is clear that when the primary field  $U_0$  interacts with the inclusion, it loses that part of its energy which is converted to scattered waves and this causes a change in the primary field. Thus, the additional field  $U_2$  must include both this change in the primary field as well as the secondary scattered waves. For instance, in the deep shadow where the total field is approximately zero, the field  $U_2$  must have a value that is close to  $-U_0$  in order to compensate for the primary field. Consequently, in the scattering diagrams of Figure 6 the forward scattered P field approaches a value of 1 at high frequencies, but this is mostly present in order to cancel the primary wave so that the total field present in this region is actually quite small. In the case of the scattering cross sections of Figure 7 this same phenomenon causes the scattered P field to approach an asymptotic value of approximately 2 at high frequencies. This follows from the fact that in this frequency range the scattered field consists of two basic terms, the energy necessary to cancel the primary field in the shadow and the energy which is scattered by the sphere, and by conservation of energy these two terms must be equal to each other and equal to the incident energy which is used to normalize the cross sections. It helps in understanding this phenomenon to consider the case of a perfectly absorbing sphere, in which case there will not be any waves that are actually scattered, but the normalized scattering cross sections will still have a value of 1.

## 6. Conclusions

The results presented in this paper can be used in a number of different ways. First, the complete and exact solution for the scattering of an elastic P wave by a spherical inclusion is presented in a convenient form. The various terms of the solution can be obtained either from the analytical solutions or a stable numerical procedure. Furthermore, a simple expression is developed for estimating the number of terms required in the harmonic series solution. The results are appropriate for arbitrary non-absorbing spherical inclusions, including fluids, and for all frequencies.

The numerical results calculated for the waves scattered from a spherical inclusion display a rich variety of interesting phenomena, some of which were briefly investigated in this study. In addition to

the wavelength of the incident wave, the results depend critically upon the distance of the observation point from the scattering object. Within the shadow zone the waves which dominate the solution near the scatterer are quite different from those that dominate at larger distances. The solutions for low velocity inclusions are quite different from those for high velocity inclusions when near the scatterer, but these differences diminish at larger distances. Also, the solutions demonstrate that an inclusion can be quite effective in transforming incident P waves to scattered S waves, which may be important in the formation of seismic codas.

The results presented in this paper should also be applicable, in at least an approximate manner, for problems involving scattering from heterogeneities more complicated than a simple sphere. Scattering by a sphere serves as a canonical problem for a general class of objects with relatively simple and smooth boundaries. It is expected that many of the scattering phenomena associated with the spherical inclusion will also apply to this wider class of heterogeneities.

Finally, as mentioned in the introduction, the results of this study can serve as the starting point for an investigation of various approximations that are typically made in the interpretation of scattered seismic waves. In assessing the validity of these approximations it is important to make comparisons with the exact solutions.

#### **Appendix A - Spherical vector system**

The spherical vector system used in this paper and its application to the problems of elastodynamics were developed by G. I. Petrashen. His original papers were published many years ago and in Russian, and are not readily available today. Thus we have included a brief summary of the system and its main properties in this appendix. More information can be found in Petrashen (1945, 1949) and Korneev and Petrashen (1987).

In a spherical coordinate system  $\{r, \theta, \phi\}$  with unit vectors  $(\hat{r}, \hat{\theta}, \hat{\phi})$  the spherical vectors are defined by the expressions

$$\mathbf{Y}_{lm}^{(1)} \equiv \mathbf{Y}_{lm}^{(1)}(\theta, \phi) = \mathbf{r} \times \nabla Y_{lm}(\theta, \phi)$$

$$\mathbf{Y}_{lm}^+ \equiv \mathbf{Y}_{lm}^+(\theta, \phi) = (l+1) \hat{\mathbf{r}} Y_{lm}(\theta, \phi) - r \nabla Y_{lm}(\theta, \phi) \quad (\text{A1})$$

$$\mathbf{Y}_{lm}^- \equiv \mathbf{Y}_{lm}^-(\theta, \phi) = l \hat{\mathbf{r}} Y_{lm}(\theta, \phi) + r \nabla Y_{lm}(\theta, \phi)$$

with the usual spherical harmonics

$$Y_{lm}(\theta, \phi) = e^{im\phi} P_l^m(\cos \theta) \quad , \quad l \geq 0 \quad , \quad -l \leq m \leq l$$

where  $P_l^m(x)$  are the associated Legendre functions

$$P_l^m(x) = (1-x^2)^{\frac{m}{2}} \frac{d^{l+m}}{dx^{l+m}} \frac{(x^2-1)^l}{2^l l!} \quad , \quad (m \geq 0)$$

$$P_l^m(x) = (-1)^{|m|} \frac{(l-|m|)!}{(l+|m|)!} P_l^{|m|}(x) \quad , \quad (m < 0)$$

In a spherical coordinate system these vectors have the components

$$\begin{aligned} \mathbf{Y}_{lm}^0 &= \frac{\partial Y_{lm}}{\partial \theta} \hat{\phi} - \frac{1}{\sin \theta} \frac{\partial Y_{lm}}{\partial \phi} \hat{\theta} \\ \mathbf{Y}_{lm}^+ &= (l+1) Y_{lm} \hat{\mathbf{r}} - \frac{\partial Y_{lm}}{\partial \theta} \hat{\theta} - \frac{1}{\sin \theta} \frac{\partial Y_{lm}}{\partial \phi} \hat{\phi} \\ \mathbf{Y}_{lm}^- &= l Y_{lm} \hat{\mathbf{r}} + \frac{\partial Y_{lm}}{\partial \theta} \hat{\theta} + \frac{1}{\sin \theta} \frac{\partial Y_{lm}}{\partial \phi} \hat{\phi} \end{aligned} \quad (\text{A2})$$

In a Cartesian coordinate system the components are

$$\begin{aligned} \mathbf{Y}_{lm}^0 &= \frac{1}{2i} \left[ Y_{l,m+1} + (l+m)(l-m+1) Y_{l,m-1} \right] \hat{\mathbf{x}} \\ &\quad - \frac{1}{2} \left[ Y_{l,m+1} - (l+m)(l-m+1) Y_{l,m-1} \right] \hat{\mathbf{y}} + im Y_{l,m} \hat{\mathbf{z}} \\ \mathbf{Y}_{lm}^+ &= \frac{1}{2} \left[ Y_{l+1,m+1} - (l-m+1)(l-m+2) Y_{l+1,m-1} \right] \hat{\mathbf{x}} \\ &\quad + \frac{1}{2i} \left[ Y_{l+1,m+1} + (l-m+1)(l-m+2) Y_{l+1,m-1} \right] \hat{\mathbf{y}} + (l-m+1) Y_{l+1,m} \hat{\mathbf{z}} \\ \mathbf{Y}_{lm}^- &= -\frac{1}{2} \left[ Y_{l-1,m+1} - (l+m)(l+m-1) Y_{l-1,m-1} \right] \hat{\mathbf{x}} \\ &\quad - \frac{1}{2i} \left[ Y_{l-1,m+1} + (l+m)(l+m-1) Y_{l-1,m-1} \right] \hat{\mathbf{y}} + (l+m) Y_{l-1,m} \hat{\mathbf{z}} \end{aligned} \quad (\text{A3})$$

The spherical vectors of the system in equation (A1) are linearly independent at any point  $(\theta, \phi)$  on a spherical surface. In the space of vector functions  $\mathbf{f}(\theta, \phi)$  defined on a sphere  $\Omega$

$$0 \leq \theta \leq \pi, \quad 0 \leq \phi \leq 2\pi, \quad d\Omega = \sin\theta \, d\theta \, d\phi$$

the vectors satisfy the following orthogonality relation

$$\int_{\Omega} \mathbf{Y}_{lm}^{*(v)} \cdot \mathbf{Y}_{l_1 m_1}^{(v_1)} d\Omega = [c_{lm}^{(v)}]^{-2} \delta_{vv_1} \delta_{ll_1} \delta_{mm_1} \quad (\text{A4})$$

where the normalizing coefficients are given by the expressions

$$\begin{aligned} c_{lm}^0 &= \sqrt{\frac{2l+1}{4\pi l(l+1)} \cdot \frac{(l-m)!}{(l+m)!}} \\ c_{lm}^+ &= \sqrt{\frac{1}{4\pi(l+1)} \cdot \frac{(l-m)!}{(l+m)!}} \\ c_{lm}^- &= \sqrt{\frac{1}{4\pi l} \cdot \frac{(l-m)!}{(l+m)!}} \end{aligned} \quad (\text{A5})$$

For vector functions  $\mathbf{f}(\theta, \phi)$  with a finite norm

$$\int_{\Omega} |\mathbf{f}|^2 d\Omega \equiv \int_{\Omega} \mathbf{f}^* \cdot \mathbf{f} d\Omega < \infty$$

the system of spherical vectors in equation (A1) is complete in the sense of convergence in the mean for a generalized Fourier series expansion of  $\mathbf{f}(\theta, \phi)$

$$\mathbf{f}(\theta, \phi) = \sum_{v=0,+,-} \sum_{l=0}^{\infty} \sum_{m=-l}^l a_{lm}^{(v)} \mathbf{Y}_{lm}^{(v)}(\theta, \phi) \quad (\text{A6})$$

where

$$a_{lm}^{(v)} = [c_{lm}^{(v)}]^2 \int_{\Omega} \mathbf{Y}_{lm}^{*(v)} \cdot \mathbf{f} d\Omega \quad (\text{A7})$$

If the class of functions  $\mathbf{f}(\theta, \phi)$  possesses continuous first derivatives with respect to  $\theta$  and  $\phi$  on the sphere  $\Omega$ , then the series in equation (A6) convergences uniformly and also possesses first derivatives with respect to  $\theta$  and  $\phi$  that agree with those of the original function.

The main feature of the spherical vectors of equation (A1) is contained in their complete utilization of central symmetry when acted upon by any differential operator that is invariant to rotation. Consider an arbitrary differential operator  $L(r, \theta, \phi)$  which is invariant to rotation of the spherical coordinate system  $(r, \theta, \phi)$ . By invariant to rotation we mean that the operator  $L$  commutes with any other operator  $R$  that represents a rotation in three-dimensional space. Then, for an arbitrary function  $\psi(r)$ , possessing sufficient derivatives, we have the equality

$$L(r, \theta, \phi) \left[ \psi(r) Y_{lm}^{(\nu)}(\theta, \phi) \right] = \left[ M_{lm}^{(\nu)} \psi(r) \right] Y_{lm}^{(\nu)}(\theta, \phi) \quad , \quad \nu = (0, +, -) \quad (\text{A8})$$

where  $M_{lm}^{(\nu)}(r)$  is an operator that acts on the radial function  $\psi(r)$  only. This property together with the orthogonality relation in equation (A4) means that for a differential equation of the form

$$L(r, \theta, \phi) \mathbf{U} = 0$$

substituting an expansion of the form

$$\mathbf{U} = \sum_{\nu, l, m} \psi_{lm}^{(\nu)}(r) Y_{lm}^{(\nu)}(\theta, \phi)$$

converts the original system into a set of independent equations

$$M_{lm}^{(\nu)} \psi_{lm}^{(\nu)}(r) = 0$$

that only involve the radial functions  $\psi_{lm}^{(\nu)}(r)$ .

In many practical applications, it is necessary to know how the vector

$$\mathbf{U}_{lm} = \psi_{lm}^0(r) Y_{lm}^0 + \psi_{lm}^+(r) Y_{lm}^+ + \psi_{lm}^-(r) Y_{lm}^- \quad (\text{A9})$$

responds to the following differential operators :

$$\nabla \cdot \mathbf{U}_{lm} = \left\{ (l+1) \left[ \psi_{lm,r}^+ + \frac{(l+2)}{r} \psi_{lm}^+ \right] + l \left[ \psi_{lm,r}^- - \frac{(l-1)}{r} \psi_{lm}^- \right] \right\} Y_{lm}^0(\theta, \phi) \quad (\text{A10})$$

$$\begin{aligned} \nabla \times \mathbf{U}_{lm} = & \left[ \psi_{lm,r}^- - \frac{(l-1)}{r} \psi_{lm}^- - \psi_{lm,r}^+ - \frac{(l+2)}{r} \psi_{lm}^+ \right] Y_{lm}^0(\theta, \phi) \\ & + \frac{l}{2l+1} \left[ \psi_{lm,r}^0 - \frac{l}{r} \psi_{lm}^0 \right] Y_{lm}^+(\theta, \phi) - \frac{l+1}{2l+1} \left[ \psi_{lm,r}^0 + \frac{l+1}{r} \psi_{lm}^0 \right] Y_{lm}^-(\theta, \phi) \end{aligned} \quad (\text{A11})$$

$$\begin{aligned}
\nabla^2 \mathbf{U}_{lm} = & \left[ (l+1) \left\{ \psi_{lm,rr}^+ + \frac{2}{r} \psi_{lm,r}^+ - \frac{(l+1)(l+2)}{r^2} \psi_{lm}^+ \right\} \right. \\
& + l \left[ \psi_{lm,rr}^- - \frac{(2l-1)}{r} \psi_{lm,r}^- + \frac{(l-1)(l+1)}{r^2} \psi_{lm}^- \right] \left. \right] \frac{\mathbf{Y}_{lm}^+(\theta, \phi)}{2l+1} \\
& + \left[ (l+1) \left\{ \psi_{lm,rr}^+ + \frac{(2l+3)}{r} \psi_{lm,r}^+ + \frac{l(l+2)}{r^2} \psi_{lm}^+ \right\} \right. \\
& + l \left[ \psi_{lm,rr}^- + \frac{2}{r} \psi_{lm,r}^- - \frac{l(l-1)}{r^2} \psi_{lm}^- \right] \left. \right] \frac{\mathbf{Y}_{lm}^-(\theta, \phi)}{2l+1}
\end{aligned} \tag{A12}$$

$$\begin{aligned}
\Delta \mathbf{U}_{lm} = \nabla^2 \mathbf{U}_{lm} - \nabla \times \nabla \times \mathbf{U}_{lm} = & \left[ \psi_{lm,rr}^0 + \frac{2}{r} \psi_{lm,r}^0 - \frac{l(l+1)}{r^2} \psi_{lm}^0 \right] \mathbf{Y}_{lm}^0(\theta, \phi) \\
& + \left[ \psi_{lm,rr}^+ + \frac{2}{r} \psi_{lm,r}^+ - \frac{(l+1)(l+2)}{r^2} \psi_{lm}^+ \right] \mathbf{Y}_{lm}^+(\theta, \phi) \\
& + \left[ \psi_{lm,rr}^- + \frac{2}{r} \psi_{lm,r}^- - \frac{l(l-1)}{r^2} \psi_{lm}^- \right] \mathbf{Y}_{lm}^-(\theta, \phi)
\end{aligned} \tag{A13}$$

Finally we note that in the case of boundary conditions with cylindrical symmetry, it is convenient to use a cylindrical vector system

$$\begin{aligned}
\mathbf{Y}_m^0 &= Y_m \hat{\mathbf{z}} \\
\mathbf{Y}_m^+ &= Y_m \hat{\boldsymbol{\rho}} - i Y_m \hat{\boldsymbol{\phi}} \\
\mathbf{Y}_m^- &= Y_m \hat{\boldsymbol{\rho}} + i Y_m \hat{\boldsymbol{\phi}}
\end{aligned} \tag{A14}$$

where  $Y_m = e^{im\phi}$  and  $(\hat{\boldsymbol{\rho}}, \hat{\boldsymbol{\phi}}, \hat{\mathbf{z}})$  are unit vectors of a cylindrical coordinate system  $(\rho, \phi, z)$ . For the case of cylindrical symmetry the vector system of equation (A14) possesses the main features of the system of spherical vectors of equation (A1).

## Appendix B

The analytical solutions for the unknown coefficients in equation (2.20) are

$$a_l^{(\nu)} = \frac{\Delta_a^{(\nu)}}{\Delta}, \quad b_l^{(\nu)} = \frac{\Delta_b^{(\nu)}}{\Delta}, \quad (\nu = 1, 2) \tag{B.1}$$

where

$$\begin{aligned} \Delta = & \frac{(\eta_2 \xi_2)^3}{(2l+1)^2} \left\{ \frac{h_l(\xi_2)}{\xi_2} \frac{h_l(\eta_2)}{\eta_2} (2l+1) \Delta_1 + \frac{j_l(\xi_1)}{\xi_1} \frac{j_l(\eta_1)}{\eta_1} (2l+1) \Delta_2 \left( \frac{\rho_1}{\rho_2} \right)^2 \right. \\ & - (2l+1) \frac{\rho_1}{\rho_2} \left[ \frac{h_l(\xi_2)}{\xi_2} \frac{j_l(\eta_1)}{\eta_1} \Delta_{12} + \frac{j_l(\xi_1)}{\xi_1} \frac{h_l(\eta_2)}{\eta_2} \Delta_{21} \right] \\ & - q \Delta_1 \left[ \Delta_2 + (l+2) h_{l+1}(\xi_2) h_{l+1}(\eta_2) + (l-1) h_{l-1}(\xi_2) h_{l-1}(\eta_2) \right] \\ & \left. + q \frac{\rho_1}{\rho_2} \Delta_2 \left[ \Delta_1 + (l+2) j_{l+1}(\xi_1) j_{l+1}(\eta_1) + (l-1) j_{l-1}(\xi_1) j_{l-1}(\eta_1) \right] + q^2 (l-1)(l+2) \Delta_1 \Delta_2 \right\} \quad (B.2) \end{aligned}$$

$$\begin{aligned} \Delta_a^{(1)} = & i \eta_2^3 \left\{ \frac{h_l(\eta_2)}{\eta_2} \left[ l \left[ 1 - \frac{\rho_1}{\rho_2} - (l+2)(2l+1)q \right] \frac{j_l(\eta_1)}{\eta_1} + (l(l+2)q-1) j_{l-1}(\eta_1) \right] \right. \\ & \left. + h_{l-1}(\eta_2) \left[ \left[ \frac{\rho_1}{\rho_2} + l(l+2)q \right] \frac{j_l(\eta_1)}{\eta_1} - q j_{l-1}(\eta_1) \right] \right\} \quad (B.3) \end{aligned}$$

$$\begin{aligned} \Delta_b^{(1)} = & -i \eta_2^3 \left\{ \frac{h_l(\eta_2)}{\eta_2} \left[ \left[ 1 - \frac{\rho_1}{\rho_2} - (l+2)(2l+1)q \right] \frac{j_l(\xi_1)}{\xi_1} + (l+2)q j_{l-1}(\xi_1) \right] \right. \\ & \left. + h_{l-1}(\eta_2) q \left[ (l+2) \frac{j_l(\xi_1)}{\xi_1} - j_{l-1}(\xi_1) \right] \right\} \quad (B.4) \end{aligned}$$

$$\begin{aligned} \Delta_b^{(2)} = & i \eta_2^3 \left\{ j_{l-1}(\xi_1) j_{l-1}(\eta_1) q \left[ 1 - (l-1)(l+2)q \right] - \frac{j_l(\xi_1)}{\xi_1} \frac{j_l(\eta_1)}{\eta_1} \frac{\rho_1}{\rho_2} \left[ 1 - \frac{\rho_1}{\rho_2} - (l+2)(2l+1)q \right] \right. \\ & \left. + j_{l-1}(\xi_1) \frac{j_l(\eta_1)}{\eta_1} q \left[ l(l-1)(l+2)q - l - 2 \frac{\rho_1}{\rho_2} \right] + j_{l-1}(\eta_1) \frac{j_l(\xi_1)}{\xi_1} q \left[ (l^2-1)(l+2)q - l - 1 - \frac{\rho_1}{\rho_2} \right] \right\} \quad (B.5) \end{aligned}$$

The following relation exists between the terms in equations (B-3) - (B-5).

$$\Delta_b^{(2)} = i \operatorname{Im} \left[ \Delta_b^{(1)} \Delta_a^{(1)*} \right]$$

An expression for  $\Delta_a^{(2)}$  can be derived from equation (B.2) by substituting for functions  $h_k(\xi_2)$  ( $k = l-1, l, l+1$ ) the corresponding functions  $-j_k(\xi_2)$ . The following quantities were used in

equations (B.2) - (B.5)

$$\begin{aligned}
\Delta_1 &= (l+1) j_{l+1}(\xi_1) j_{l-1}(\eta_1) + l j_{l-1}(\xi_1) j_{l+1}(\eta_1) \\
\Delta_2 &= (l+1) h_{l+1}(\xi_2) h_{l-1}(\eta_2) + l h_{l-1}(\xi_2) h_{l+1}(\eta_2) \\
\Delta_{12} &= (l+1) j_{l+1}(\xi_1) h_{l-1}(\eta_2) + l j_{l-1}(\xi_1) h_{l+1}(\eta_2) \\
\Delta_{21} &= (l+1) h_{l+1}(\xi_2) j_{l-1}(\eta_1) + l h_{l-1}(\xi_2) j_{l+1}(\eta_1) \\
q &= \frac{2}{\eta_2^2} \left[ 1 - \frac{\rho_1 \eta_2^2}{\rho_2 \eta_1^2} \right] = \frac{2}{\eta_2^2} \left[ 1 - \frac{\mu_1}{\mu_2} \right]
\end{aligned} \tag{B.6}$$

For the case of a fluid within the sphere, the above equations can still be used provided the following substitutions are made:

$$\mu_1 = 0, \quad j_{l+1}(\eta_1) = 1, \quad j_{l-1}(\eta_1) = -1, \quad j_l(\eta_1) = 0 \tag{B.7}$$

$$\begin{aligned}
\Delta &= \frac{\eta_2^2 \xi_2^3}{2l+1} \left\{ (2l+1) \frac{h_l(\xi_2)}{\xi_2} h_l(\eta_2) \left[ j_{l+1}(\xi_1) - \frac{l}{\xi_1} j_l(\xi_1) \right] \right. \\
&\quad \left. - (2l+1) \frac{\rho_1}{\rho_2} \frac{j_l(\xi_1)}{\xi_1} h_l(\eta_2) \left[ h_{l+1}(\xi_2) - \frac{l}{\xi_2} h_l(\xi_2) \right] \right. \\
&\quad \left. - \frac{2}{\eta_2} \left[ j_{l+1}(\xi_1) - \frac{l}{\xi_1} j_l(\xi_1) \right] \left[ \Delta_2 + (l+2) h_{l+1}(\xi_2) h_{l+1}(\eta_2) + (l-1) h_{l-1}(\xi_2) h_{l-1}(\eta_2) \right] \right. \\
&\quad \left. + \frac{2}{\eta_2} \frac{\rho_1}{\rho_2} \Delta_2 \left[ 2j_{l+1}(\xi_1) - \frac{2l-1}{\xi_1} j_l(\xi_1) \right] + \frac{4}{\eta_2^3} (l-1)(l+2) \Delta_2 \left[ j_{l+1}(\xi_1) - \frac{l}{\xi_1} j_l(\xi_1) \right] \right\} \tag{B.8}
\end{aligned}$$

$$\Delta_a^{(1)} = i \eta_2^2 \left\{ h_l(\eta_2) + \frac{2}{\eta_2} \left[ (l^2-1) \frac{h_l(\eta_2)}{\eta_2} - h_{l+1}(\eta_2) \right] \right\} \tag{B.9}$$

$$\Delta_b^{(1)} = 0 \tag{B.10}$$

$$\Delta_b^{(2)} = -2i \eta_2 \left\{ j_{l-1}(\xi_1) \left[ 1 - (l-1)(l+2)q \right] + \frac{j_l(\xi_1)}{\xi_1} \left[ (l^2-1)(l+2)q - l - 1 - \frac{\rho_1}{\rho_2} \right] \right\} \tag{B.11}$$

An expression for  $\Delta_a^{(2)}$  can be derived from the one for  $\Delta$  in the same way as for the elastic case.



## Acknowledgements

This research was supported by Phillips Laboratory under Contract F19628-90-K-0055 and also by the U.S. Department of Energy under Contract DE-AC03-76SF00098.

## References

- Aki, K., 1969. Analysis of the seismic coda of local earthquakes as scattered waves, *J. Geophys. Res.*, **74**, 615-631.
- Aki, K., 1973. Scattering of P-waves under the Montana LASA, *J. Geophys. Res.*, **79**, 1334-1346.
- Aki, K., 1980. Scattering and attenuation of shear waves in the lithosphere, *J. Geophys. Res.*, **85**, 6469-6504.
- Buldyrev, V. S., 1964. Diffraction of waves by a transparent sphere, - Numerical methods of solution of differential and integral equations and integral formulas, *Scientific Papers of Leningrad State University, Series in Mathematical Sciences*, 287-291.
- Buldyrev, V. S., and Molotkov, I. A., 1960. Investigation of exact solutions of unharmonic diffraction problems near the wavefronts of slide waves, *Doklady Acad. Nauk USSR*, **134**, 1051-1054.
- Buldyrev, V. S., and Molotkov, I. A., 1958. About the unharmonic propagation of waves in homogeneous and isotropic media with cylindrical and spherical boundaries, *Scientific Papers of Leningrad State University, Series in Mathematical Sciences*, **246**, 261-321.
- Clebsch, A., 1863. Über die reflexion an einer kugelfläche, *Crelle's J. Reine Angew. Math.*, **61**, 195.
- Einspruch, N. G., Witterholt, E. J., and Truell, R., 1960. Scattering of a plane transverse wave by a spherical obstacle in an elastic medium, *J. Appl. Phys.*, **31**, 806-818.
- Gelchinskij, B. J., 1958. Some problems of wave propagation inside a homogeneous isotropic elastic sphere, *Scientific Papers of Leningrad State University, Series in Mathematical Sciences*, **246**, 322-345.
- Gubernatis, J. E., Domany, E., and Krumhansl, J. A., 1977a. Formal aspects of the theory of the scattering of ultrasound by flaws in elastic materials, *J. Appl. Phys.*, **48**, 2804-2811.

- Gubernatis, J. E., Domany, E., Krumhansl, J. A., and Huberman, M., 1977b. The Born approximation in the theory of the scattering of elastic waves by flaws, *J. Appl. Phys.*, **48**, 2812-2819.
- Haddon, R. A., and Cleary, J. R., 1974. Evidence for scattering of seismic PKP waves near the mantle-core boundary, *Phys. Earth and Planet. Int.*, **8**, 211-234.
- Hudson, J. A., 1977. Scattered waves in the coda of P, *J. Geophys.*, **43**, 359-374.
- Hudson, J. A. and Heritage, J. R., 1981. The use of the Born approximation in seismic scattering problems, *Geophys. J. R. Astr. Soc.*, **66**, 221-240.
- Korneev, V. A., 1983. About the calculation of eigenfrequencies of a radially-inhomogeneous elastic sphere, *Problems of dynamic theory of seismic wave propagation*, **23**, 26-44, Nauka, Leningrad.
- Korneev, V. A., and Petrashen, G. I., 1987. Calculation of diffraction wave fields formed on an elastic sphere, *Problems of dynamic theory of seismic wave propagation*, **27**, 26-44, Nauka, Leningrad.
- Korneev, V. A. and L. R. Johnson, L. R., 1992. Scattering of elastic waves by a spherical inclusion - 2. Limitations of asymptotic solutions, *Geophys. J. Int.*, submitted.
- Miles, J. W., 1960. Scattering of elastic waves by small inhomogeneities, *Geophysics*, **15**, 642-648.
- Morochnik, V. S., 1983. Scattering of compressional elastic waves by a low-contrast spherical inclusion, *Izvestia Acad. Nauk USSR, Fizika Zemli*, **7**, 322-345.
- Morse, P. M. and Feshbach, H., 1953. *Methods of Theoretical Physics*, McGraw-Hill, New York, 1978 pp.
- Nigul, U. K. et al., 1974. *Echo-signals from elastic objects. Part 2*, Academy of Science of Estonian SSR, Tallinn, 345 pp.
- Pao, Y.-H., and Mow, C. C., 1973. *Diffraction of Elastic Waves and Dynamic Stress Concentrations*, Crane Russak, New York, 694 pp.
- Petrashen, G.I., 1945. Solution of vector boundary problems of mathematical physics in the case of a sphere, *Doklady Acad. Nauk USSR*, **46**, No. 7.
- Petrashen, G.I., 1946. Formation of oscillations and the phenomena of resonance in the case of a sphere, *Doklady Acad. Nauk USSR*, **51**, No. 1.

- Petrashen, G.I., 1949. Symmetry of rotation and spherical vectors, *Scientific Papers of Leningrad State University, Series in Mathematical Sciences*, **114**, 3-27.
- Petrashen, G. I., 1950a. Dynamic problem of the theory of elasticity in the case of an isotropic sphere, *Scientific Papers of Leningrad State University, Series in Mathematical Sciences*, **135**, 24-70.
- Petrashen, G. I., 1950b. Oscillations of an isotropic elastic sphere. *Doklady Acad. Nauk USSR*, **47**, No. 3.
- Petrashen, G. I., 1953. Methods of investigation of wave propagation in media with spherical and cylindrical boundaries, *Scientific Papers of Leningrad State University, Series in Mathematical Sciences*, **170**, 27.
- Rayleigh, Lord, 1871. On the scattering of light by small particles, *Phil. Mag.*, **41**, 447.
- Truell, R., Elbaum, C., and Chick, B. B., 1969. *Ultrasonic Methods in Solid State Physics*, Academic Press, New York.
- Varatharajulu, V., and Pao, Y.-H., 1976. Scattering matrix for elastic waves. I. Theory, *J. Acoust. Soc. Am.*, **60**, 556-566.
- Waterman, P. C., 1976. Matrix theory of elastic wave scattering, *J. Acoust. Soc. Am.*, **60**, 567-580.
- Ying, C. F. and Truell, R., 1956. Scattering of a plane longitudinal wave by a spherical obstacle in an isotropically elastic solid, *J. Appl. Phys.*, **27**, 1086-1097.

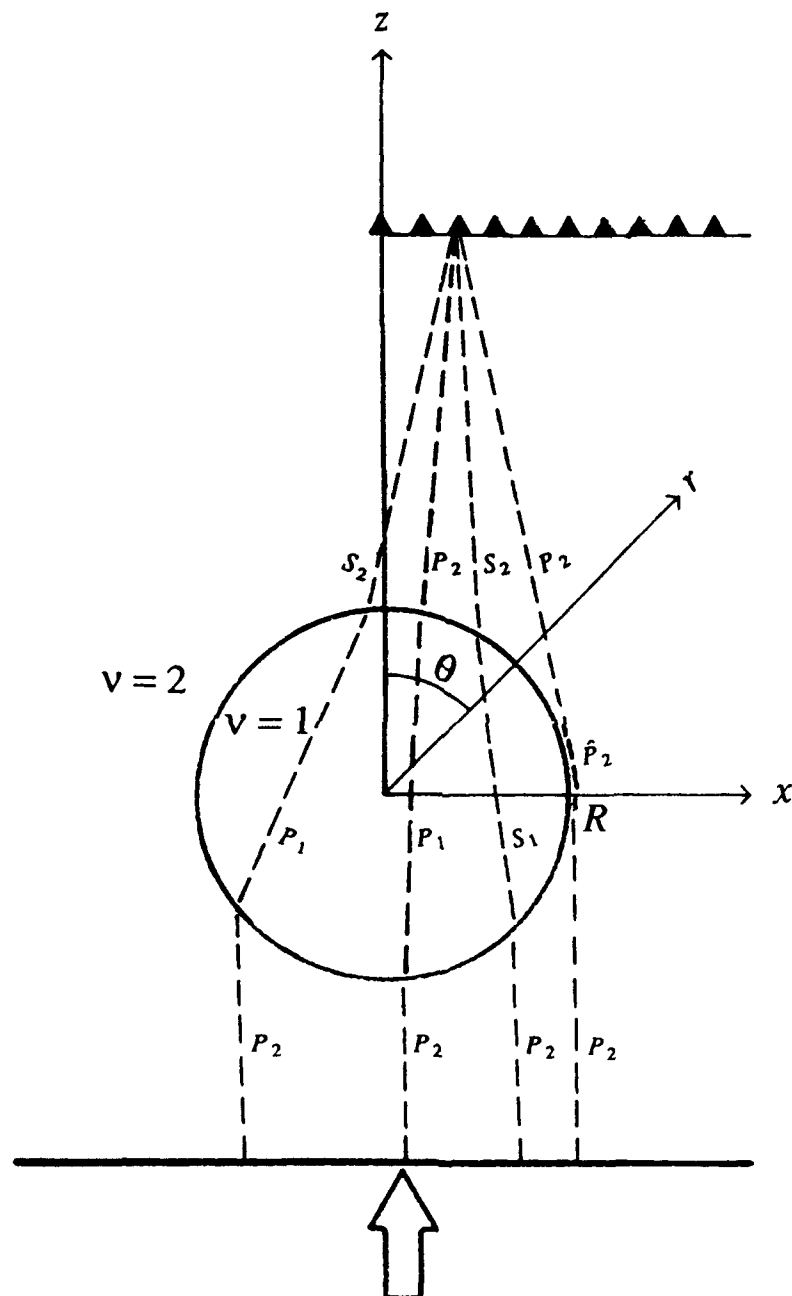


**Figure 1.** The geometry of the problem. The sphere of radius  $R$  has material properties denoted by  $v = 1$ , while the material properties of the surrounding medium are denoted by  $v = 2$ . A plane P wave is incident from along the negative  $z$  axis. The transmitted wave field is observed as a function of the  $x$  coordinate along a line that is offset a distance  $z$  from the center of the sphere.

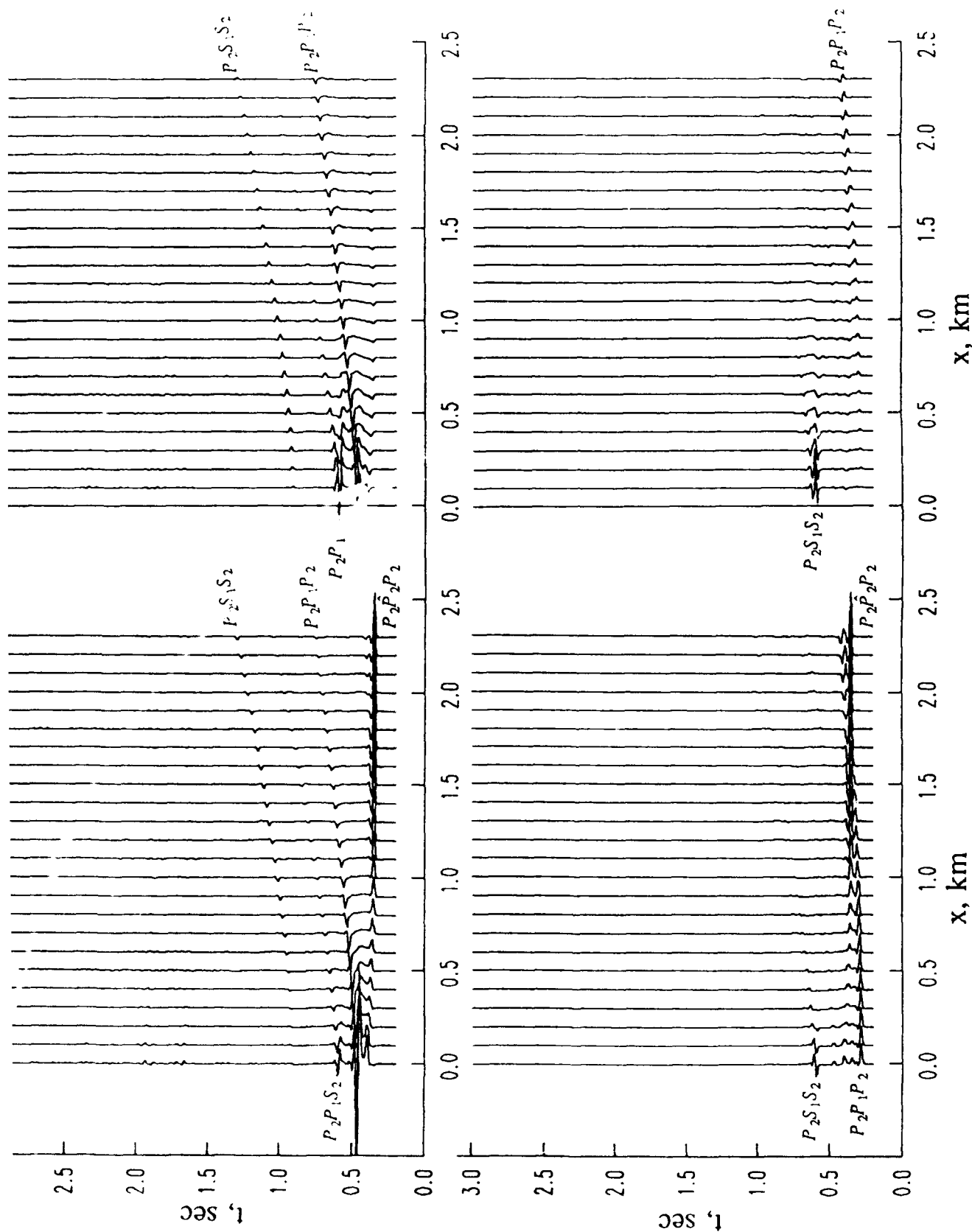


**Figure 2.** Transmitted wave fields as a function of distance  $x$  from the center of the sphere along a line that has an offset distance  $z$  of 2 km from the center of a sphere having a radius  $R = 1$  km (see Figure 1 for geometry). The panels on the left are for the  $z$  components of motion and the panels on the right are for the  $x$  components of motion. The top two panels are for model 1 of a low velocity inclusion, and the bottom two panels are for model 2 of a high velocity inclusion. The distance  $x = 1$  corresponds to the edge of the geometrical shadow

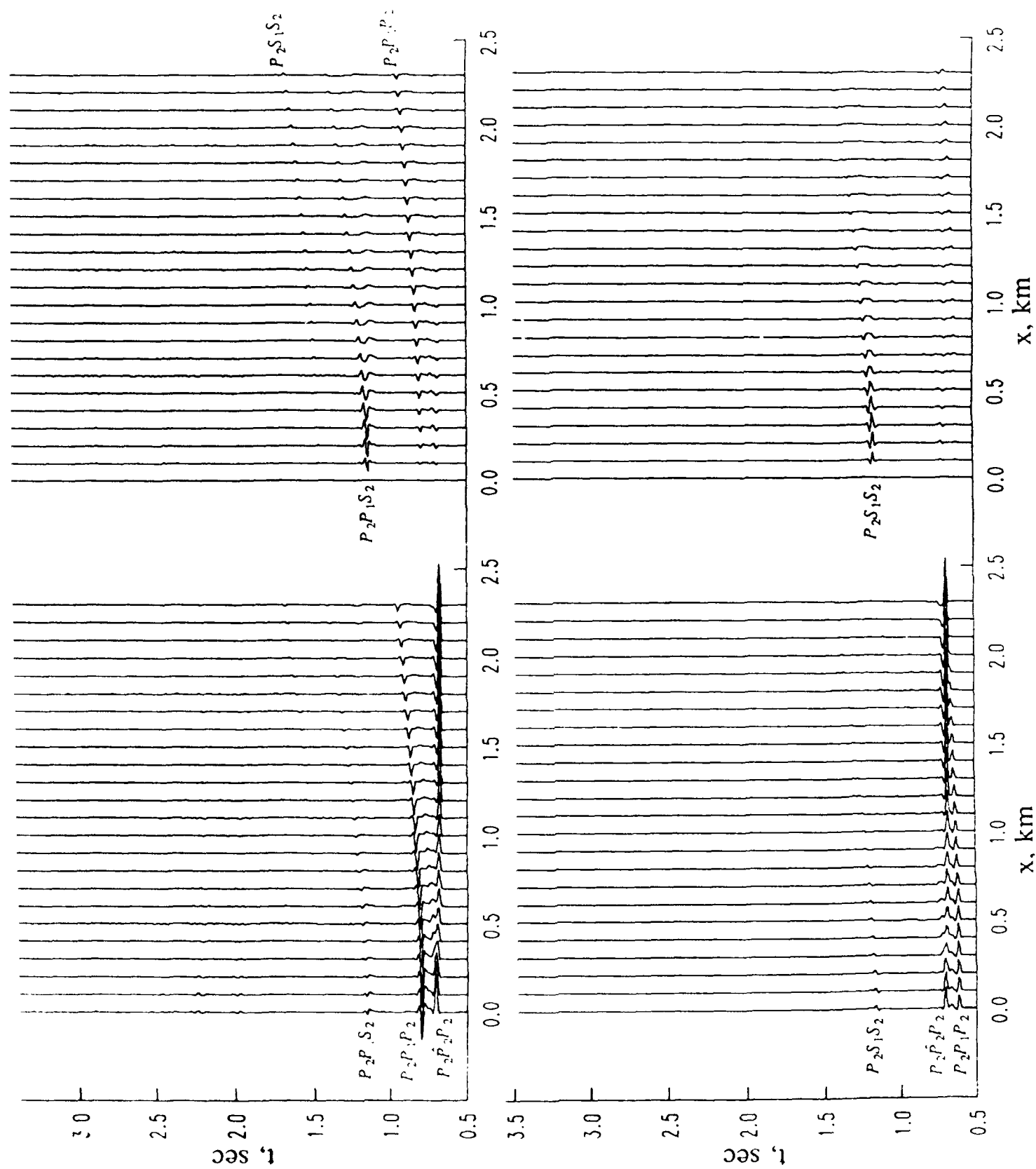


Figure 3. Similar to Figure 2 except that the offset distance  $x$  is 4 km

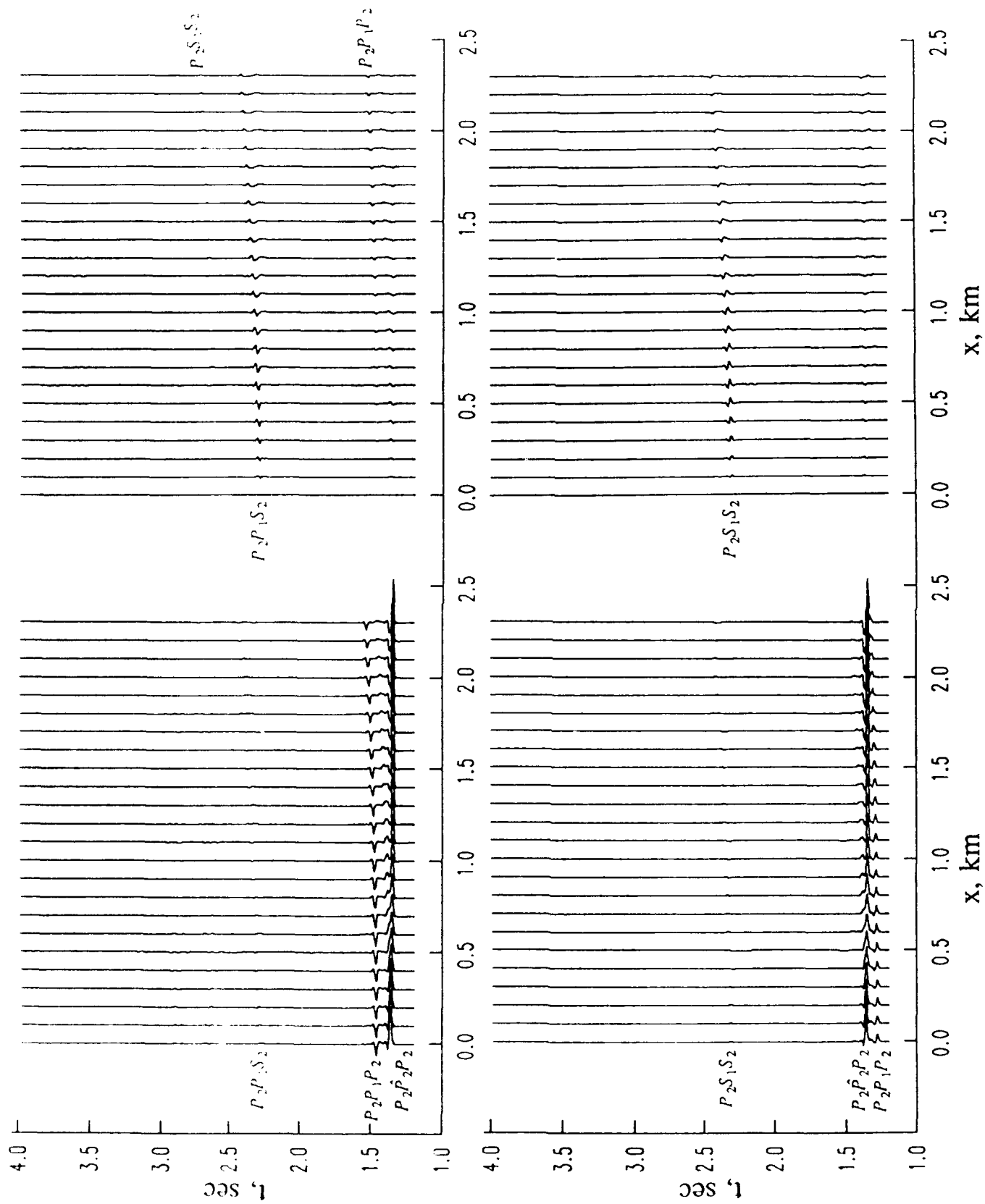
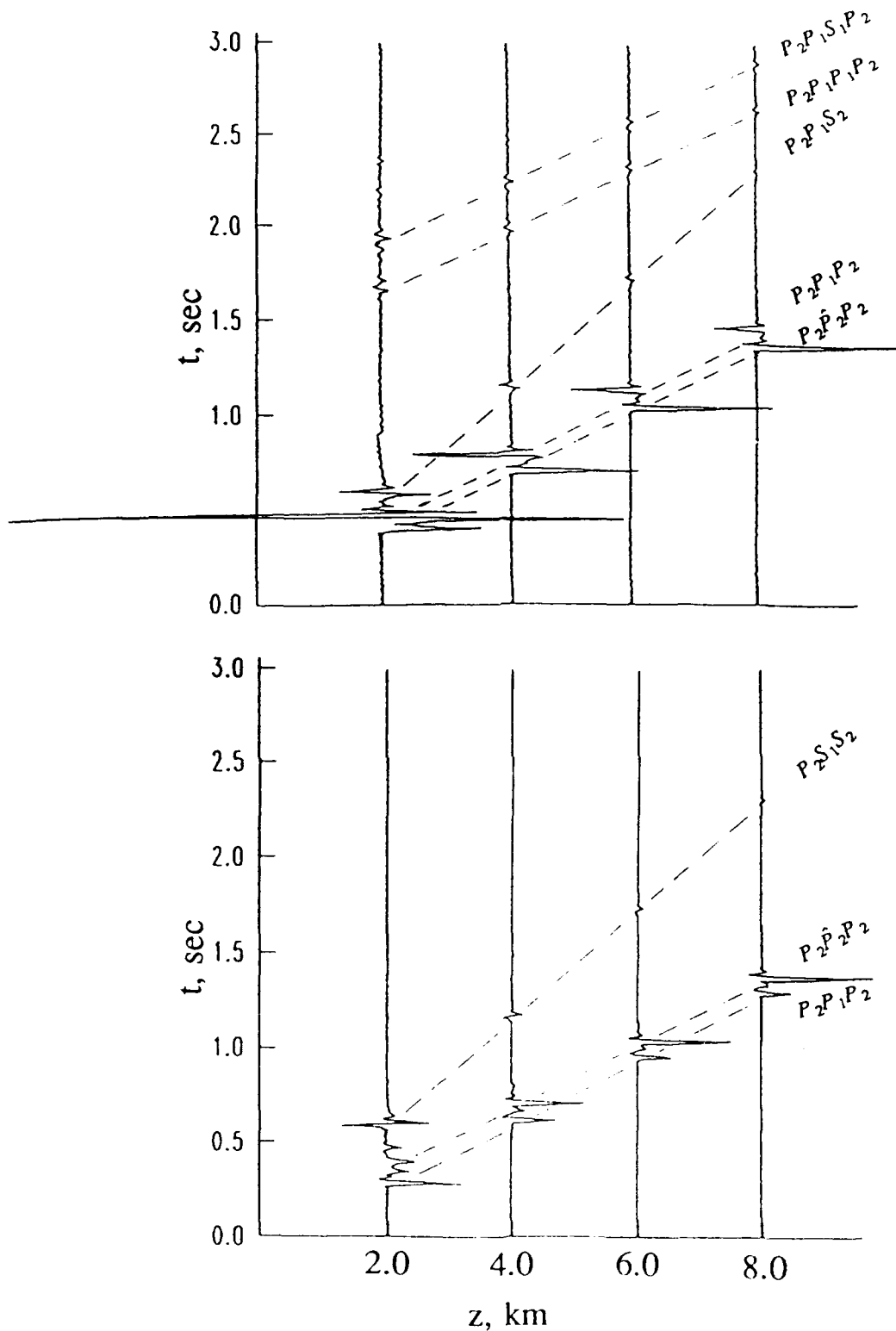
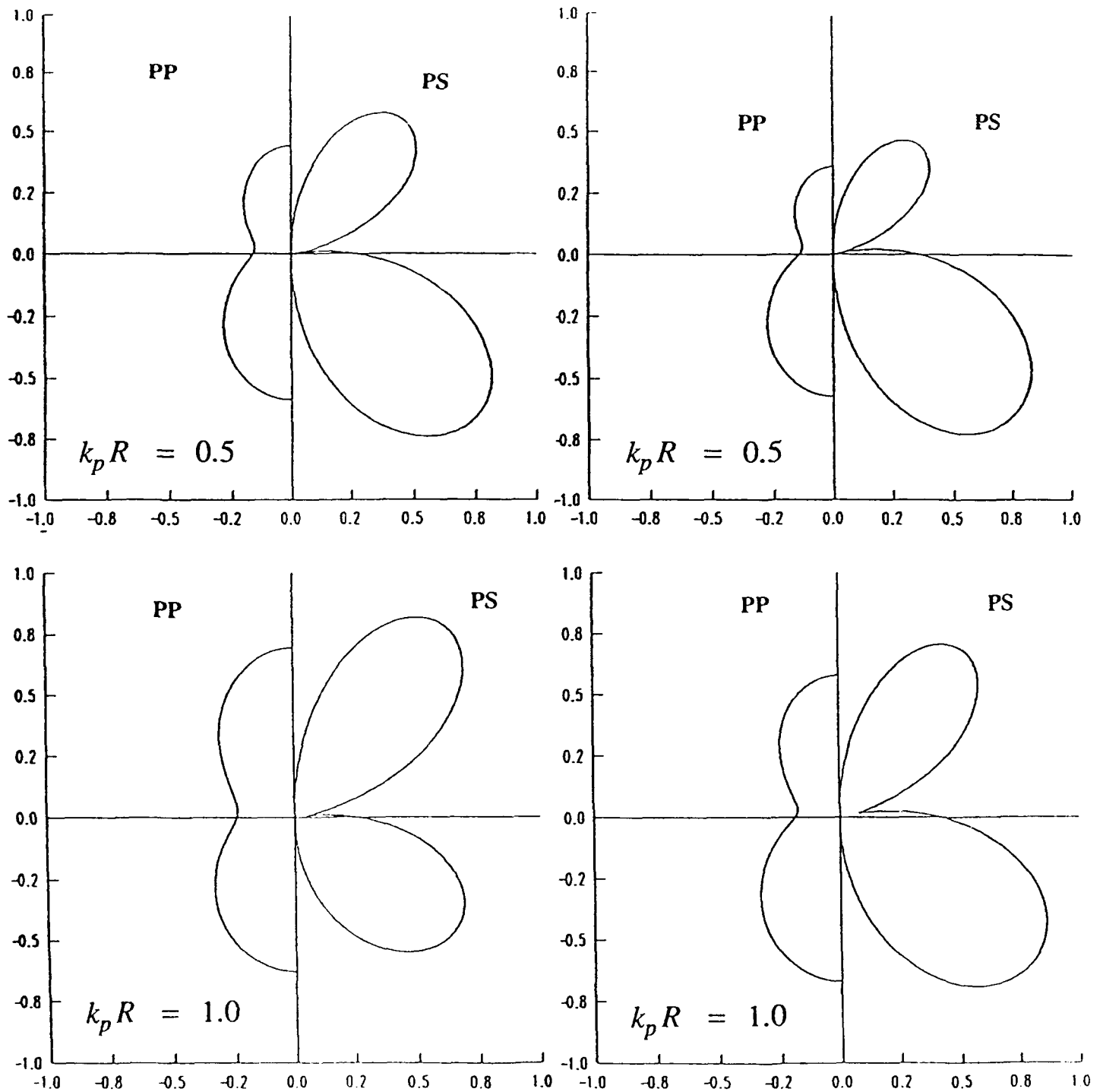


Figure 4. Similar to Figure 2 except that the offset distance  $z$  is 8 km.



**Figure 5.** Transmitted wave fields in the deepest shadow of the sphere ( $x = 0$ ) as a function of the offset distance  $z$ . Only the  $z$  component of the field is shown, as the  $x$  component is identically zero. The upper panel is for model 1 of a low velocity inclusion, and the lower panel is for model 2 of a high velocity inclusion.





**Figure 6a.** Scattering diagrams for various values of the parameter  $k_p R = \omega R / V_p$ . In each panel the left hand figure represents the scattered P field, while the right hand figure represents the scattered S field. The top two panels are for the case  $k_p R = 0.5$  and the bottom two panels are for the case  $k_p R = 1.0$ . The two panels on the left are for model 1 of a low velocity inclusion, and the two panels on the right are for model 2 of a high velocity inclusion.

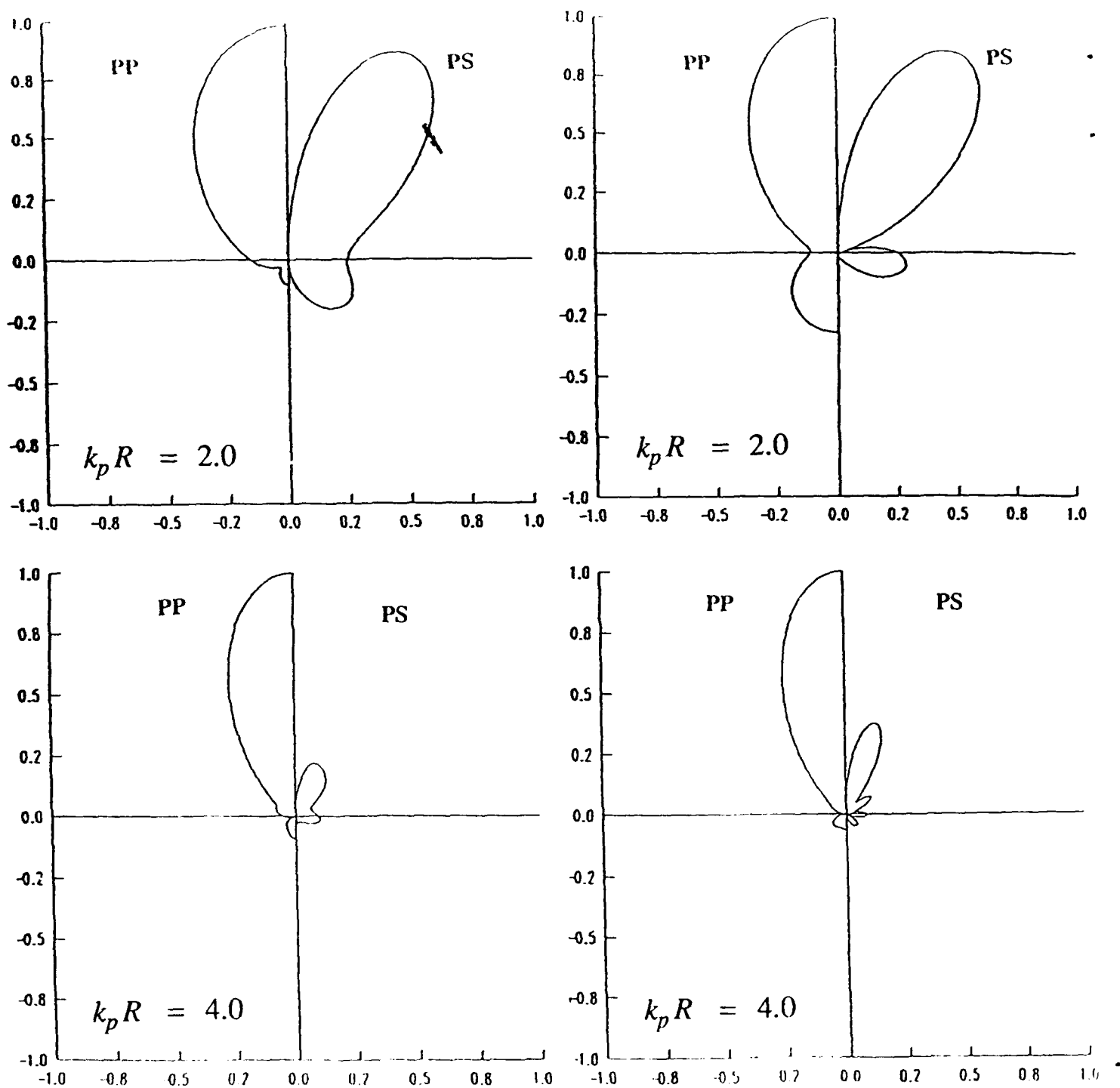


**Figure 6b.** Similar to Figure 6a except that the cases are for  $k_p R = 2$  in the top two panels and for  $k_p R = 4$  in the bottom two panels.

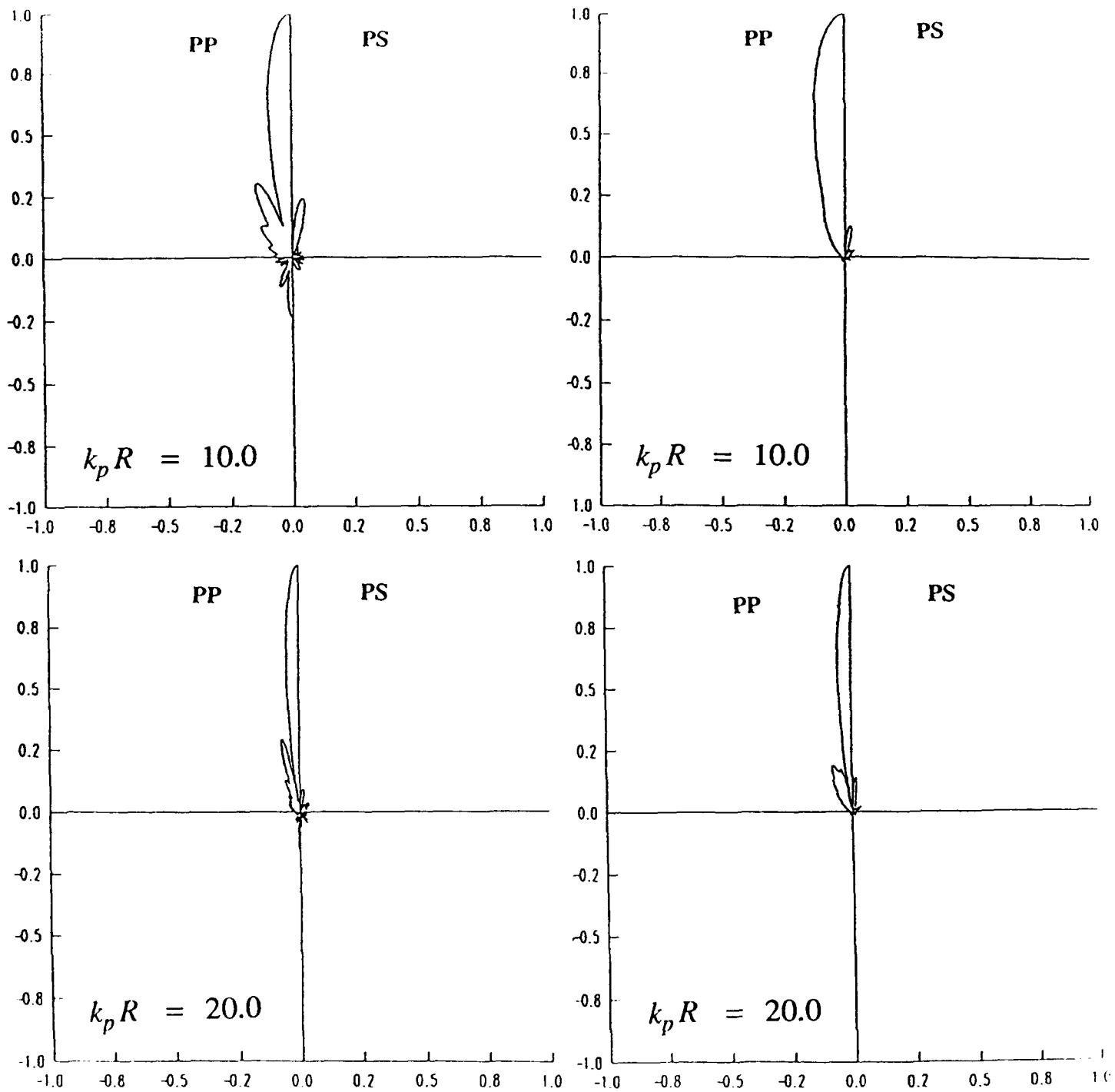


**Figure 6c.** Similar to Figure 6a except that the cases are for  $k_p R = 10$  in the top two panels and for  $k_p R = 20$  in the bottom two panels.

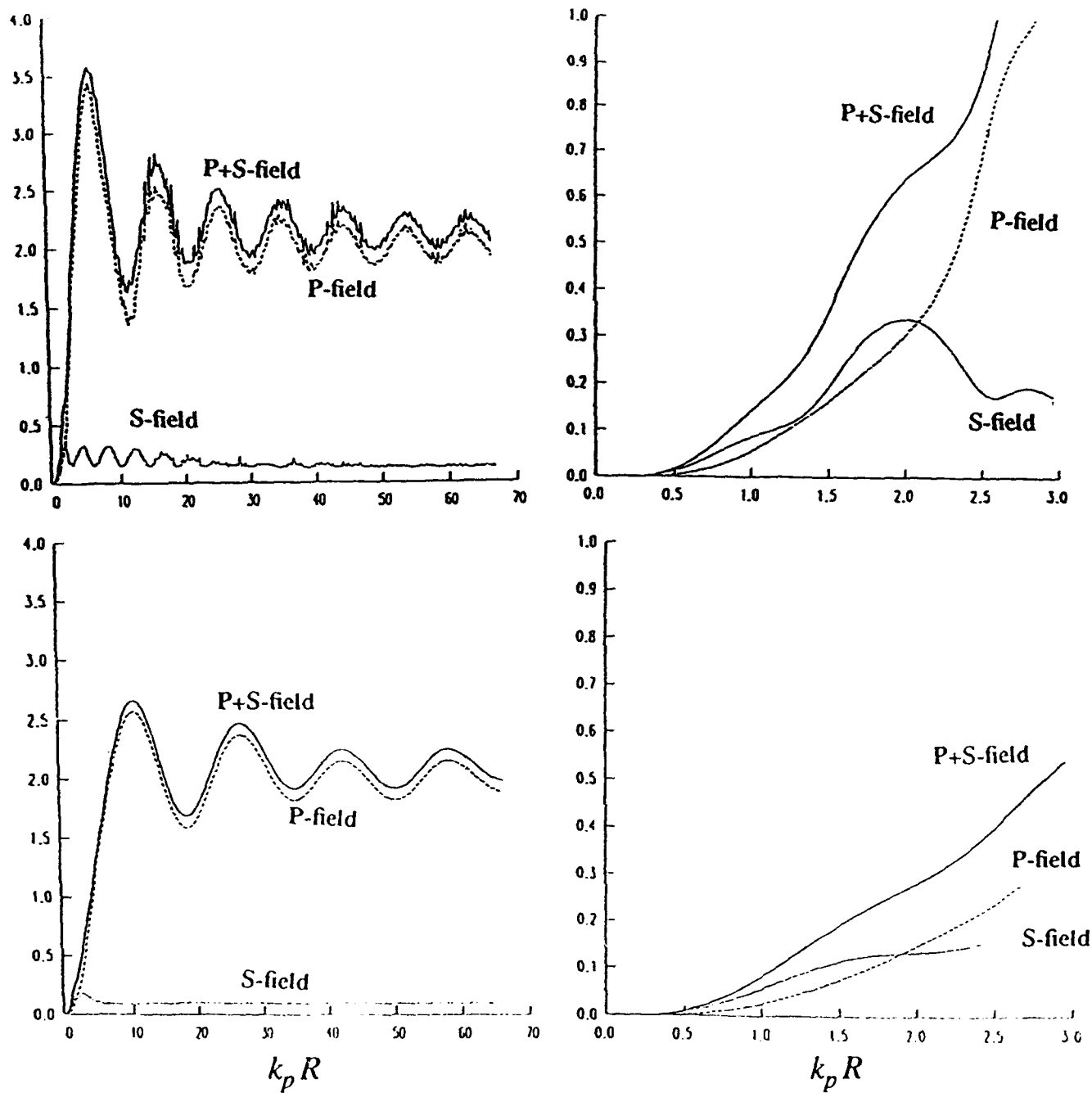


**Figure 7.** Normalized scattering cross sections as a function of the parameter  $k_p R = \omega R / V_p$ . The top two panels are for model 1 of a low velocity inclusion, and the bottom two panels are for model 2 of a high velocity inclusion. The panels on the right are expanded versions of those on the left for small values of the argument.

## **Scattering of elastic waves by a spherical inclusion - 2. Limitations of asymptotic solutions**

*Valeri A. Korneev and Lane R. Johnson*

Department of Geology and Geophysics, University of California,  
and Center for Computational Seismology, Lawrence Berkeley Laboratory,  
Berkeley, California 94720

Starting with the exact solution for the scattering of a plane P wave by a homogeneous spherical inclusion, various types of approximate solutions are developed and discussed. The standard Rayleigh and Mie approximations are extended to the case of inclusions having arbitrary contrasts in material properties. For the low contrast case, solutions are developed which are valid over a wide frequency range. Several aspects of these solutions are discussed, including the importance of near-field terms and the relative strength of the scattered P and S fields. The various types of approximate solutions are compared with each other and with the exact solution by calculating and displaying their normalized scattering cross sections.

**Key words:** elastic waves, sphere, scattering, diffraction

### **1. Introduction**

Scattering of seismic waves plays a significant role in seismic wave propagation in the earth. Such phenomena as coda wave excitation, attenuation, precursors, and irregular arrival times are often assumed to be caused by scattering from inhomogeneities of the earth's crust and upper mantle. The scattering mechanism also plays a role in some of the algorithms for migration and diffraction tomography which are used in exploration seismology.

Exact solutions for scattering problems are known for only a few types of obstacles, and even for these cases the calculations are not easily implemented because of their complicated mathematical representations. The basic approach to the scattering problem which has been developed in such disciplines

as optics, acoustics, and quantum mechanics makes extensive use of asymptotic solutions to explain the main physical features of the scattered fields. In these disciplines, where the critical parameters of the scattering obstacle and the observation system are usually well known and controllable, experiments can be arranged so that the conditions for the asymptotic solutions are strongly satisfied, and thus these solutions give a satisfactory representation of the observational results. However, in the case of scattered seismic waves the situation is more complicated. Generally there is a wide variety of shapes, locations, boundaries, and material properties in the local heterogeneity of the earth's crust and upper mantle which represent the scattering obstacles for the seismic problem. Additional complications arise from the fact that these local heterogeneities are measured with respect to a surrounding material which is itself typically inhomogeneous, but on a larger distance scale. In most cases the parameters of the scattering obstacles are either unknown or poorly known. Furthermore, parameters of the observation system, such as the locations of the sources and receivers and the wavelengths of the incident waves, are typically difficult to control. Therefore, a common situation in seismic problems is that it is unknown whether the conditions necessary for the application of asymptotic solutions are actually satisfied.

Establishing proper conditions for the use of different asymptotic approaches in the treatment of scattered seismic waves is not a simple problem because of a number of reasons:

1. The broad range in the type and size of scattering obstacles which have to be considered makes it difficult to find an asymptotic approach which is applicable over the entire range.
2. The fact that several different parameters are involved, some of which are poorly known, makes it difficult to ascertain whether an asymptotic solution is appropriate or not.
3. It is often necessary to apply a combination of asymptotic solutions and some of these may be incompatible. For example, for the far field ( $r \rightarrow \infty$ ) solution in the case of the Rayleigh approximation ( $\omega \rightarrow 0$ ) there is the possibility of a contradiction, because the parameter  $kr = \omega r/V$  is assumed to be large.
4. The absence of a set of canonical problems for which exact solutions are known makes it impossible to check the asymptotic solutions by comparing them with the exact solutions.

In the present paper we consider various asymptotic representations of the scattered fields formed when a plane P-wave is incident on an elastic spherical inclusion. An exact solution for this problem and methods of calculating it were developed in a previous paper (Korneev and Johnson, 1992). This exact solution can be used as the starting point for some of the asymptotic solutions. It can also be compared with the asymptotic solutions as a means of investigating their validity.

## 2. Solutions for small inclusions

We begin with a brief review of some of the approximate scattering solutions that are commonly used in seismology. Consider an elastic medium with an inclusion at the center of joint Cartesian  $(x, y, z)$  and spherical  $(r, \theta, \phi)$  coordinate systems. The parameters within the inclusion, denoted by the index  $(v = 1)$ , are allowed to be functions of the coordinates

$$\lambda_1 = \lambda_1(x, y, z) \quad , \quad \mu_1 = \mu_1(x, y, z) \quad , \quad \rho_1 = \rho_1(x, y, z) \quad (1)$$

The volume of the inclusion will be denoted by  $V$ . The surrounding media, denoted by the index  $v = 2$  and described by the constant parameters

$$\lambda_2 \equiv \lambda = \text{const.} \quad , \quad \mu_2 \equiv \mu = \text{const.} \quad , \quad \rho_2 = \rho = \text{const.} \quad (2)$$

is assumed to be homogeneous. In the equations that follow, material constants without indexes refer to the surrounding media ( $v=2$ ).

Most of the approximate solutions used in seismology involve the Born approximation, which is assumed to be valid in the case of weak single scattering (Aki and Chouet, 1975; Sato, 1984; Wu and Aki, 1985a, 1985b). The actual conditions under which the Born approximation is valid are rather complicated and involve both the dimensions of the inclusion and the contrast in its material properties (Hudson and Heritage, 1981), but it is commonly assumed in seismology that they are equivalent to the condition of a small contrast in material properties. By this we mean that the perturbations of the elastic parameters within the inclusion are small in comparison with those in the surrounding medium

$$\frac{|\delta\lambda|}{\lambda} = \frac{|\lambda_1 - \lambda_2|}{\lambda_2} \ll 1, \quad \frac{|\delta\mu|}{\mu} = \frac{|\mu_1 - \mu_2|}{\mu_2} \ll 1, \quad \frac{|\delta\rho|}{\rho} = \frac{|\rho_1 - \rho_2|}{\rho_2} \ll 1 \quad (3)$$

Throughout this paper we will be considering an incident plane P wave of the form

$$\tilde{U}_0 = e^{i\omega(t - \frac{z}{V_p})} \hat{z} = U_0 e^{i\omega z} \quad (4)$$

This wave is traveling along the z axis in the positive direction. The solution to the scattering problem, which includes both the incident and scattered fields, will be written as

$$\tilde{U} = U e^{i\omega z} = (U_0 + U_p + U_s) e^{i\omega z} \quad (5)$$

where  $U_p$  and  $U_s$  represent the scattered P and S waves, respectively.

Our next approximation is to consider the solution at low frequencies. Then only the first members of the frequency power series are retained and the solution is

$$U_p = A \left\{ -\frac{\delta\lambda}{\lambda + 2\mu} + \frac{\delta\rho}{\rho} \cos\theta - \frac{2\delta\mu}{\lambda + 2\mu} \cos^2\theta \right\} \hat{r} \quad (6a)$$

$$U_s = B \left\{ -\frac{\delta\rho}{\rho} \sin\theta + \gamma \frac{\delta\mu}{\mu} \sin 2\theta \right\} \hat{\theta} \quad (6b)$$

and where the following definitions have been used

$$A = k_p^2 \frac{V}{4\pi} \frac{e^{-ik_p r}}{r}, \quad B = k_s^2 \frac{V}{4\pi} \frac{e^{-ik_s r}}{r}, \quad k_p = \frac{\omega}{V_p}, \quad k_s = \frac{\omega}{V_s} \quad (7)$$

$$V_p^{(v)} = \sqrt{\frac{\lambda_v + 2\mu_v}{\rho_v}}, \quad V_s^{(v)} = \sqrt{\frac{\mu_v}{\rho_v}}, \quad \gamma = \frac{V_s}{V_p} \quad (8)$$

The above result has used only the first term in a power series of frequency and is thus dependent upon the assumption that

$$k_p \bar{R} = \frac{\omega \bar{R}}{V_p} \ll 1 \quad (9)$$

where  $\bar{R}$  is the average radius of the inclusion. This is generally known as the Rayleigh-Born approximation. The solution of equation (6) obviously does not depend upon the shape of the inclusion, but only upon its volume. Thus, for the case of Rayleigh scattering, all parts of a homogeneous inclusion contribute in proportion to their volume and the scattered field is a simple sum of these contributions.



When the wavelength of the incident wave is comparable to the size of the inclusion and equation (9) is no longer valid, then a different approximation must be used. In Mie scattering the phase differences of the incident wave for different parts of inclusion are taken into account (Chernov, 1960). The solution is

$$U_p = A \int_V \left[ -\frac{\delta\lambda(\xi)}{\lambda + 2\mu} + \frac{\delta\rho(\xi)}{\rho} \cos\theta - \frac{2\delta\mu(\xi)}{\lambda + 2\mu} \cos^2\theta \right] e^{-i\omega S_1 \xi} dV(\xi) \hat{r} \quad (10a)$$

$$U_s = B \int_V \left[ -\frac{\delta\rho(\xi)}{\rho} \sin\theta + \gamma \frac{\delta\mu(\xi)}{\mu} \sin 2\theta \right] e^{-i\omega S_2 \xi} dV(\xi) \hat{\theta} \quad (10b)$$

where

$$S_1 = V_p^{-1} \hat{z} - V_p^{-1} \hat{r} \quad S_2 = V_p^{-1} \hat{z} - V_s^{-1} \hat{r}$$

$$S_1 = |S_1| = 2V_p^{-1} \sin \frac{\theta}{2} \quad S_2 = |S_2| = \sqrt{V_p^{-2} + V_s^{-2} - 2V_p^{-1} V_s^{-1} \cos\theta}$$

This approximation is equivalent to assuming that the inclusion is composed of numerous small noninteracting parts, each of which causes a scattered field of the form of equation (6).

For the case where the scattering volume is a homogeneous sphere of radius  $R$ , the expressions in equation (10) can be integrated to give

$$U_p = A \left\{ -\frac{\delta\lambda}{\lambda + 2\mu} + \frac{\delta\rho}{\rho} \cos\theta - \frac{2\delta\mu}{\lambda + 2\mu} \cos^2\theta \right\} \frac{j_1(q_1)}{q_1} \hat{r} \quad (11a)$$

$$U_s = B \left\{ -\frac{\delta\rho}{\rho} \sin\theta + \gamma \frac{\delta\mu}{\mu} \sin 2\theta \right\} \frac{j_1(q_2)}{q_2} \hat{\theta} \quad (11b)$$

where

$$q_1 = \omega S_1 R \quad \text{and} \quad q_2 = \omega S_2 R$$

and  $j_l(q)$  is the spherical Bessel function of order  $l$ .

The solutions of equations (6) and (10) have been used in many publications for estimating seismic attenuation, explaining the generation of coda waves, obtaining high-frequency asymptotics, and formulating seismic diffraction tomography. In most of these applications, however, valid bounds on the relevant parameters are not established, and possible errors due to the use of asymptotic solutions are not

considered. As a result, large errors in the estimated seismic parameters may occur, or invalid solutions may be produced. In a later section we will illustrate these possibilities by comparing the approximate solutions of equations (6) and (10) with the exact solution for a homogeneous elastic sphere.

### 3. Exact solution for the sphere

A method of calculating the exact scattering solution for a homogeneous elastic sphere was presented in detail in a previous paper (Korneev & Johnson, 1992), so the results will only be summarized here. The solution for the medium outside of the sphere for the case of an incident plane P wave has the form

$$\mathbf{U} = \mathbf{U}_0 + \mathbf{U}_2 \quad (12)$$

where

$$\begin{aligned} \mathbf{U}_2 = \mathbf{U}_p + \mathbf{U}_s &= \sum_{l \geq 0} \left\{ \left[ a_l h_{l+1}(k_p r) + l b_l h_{l+1}(k_s r) \right] \mathbf{Y}_{l0}^+ \right. \\ &\quad \left. + \left[ -a_l h_{l-1}(k_p r) + (l+1) b_l h_{l-1}(k_s r) \right] \mathbf{Y}_{l0}^- \right\} e^{-i \frac{\pi}{2} (l+1)} \\ &= \sum_{l \geq 0} e^{-i \frac{\pi}{2} (l+1)} (2l+1) \left\{ a_l \left[ \left[ (l+1) \frac{h_l(k_p r)}{k_p r} - h_{l-1}(k_p r) \right] P_l(\cos \theta) \hat{\mathbf{r}} - \frac{h_l(k_p r)}{k_p r} \frac{\partial P_l(\cos \theta)}{\partial \theta} \hat{\boldsymbol{\theta}} \right] \right. \\ &\quad \left. + b_l \left[ l(l+1) \frac{h_l(k_s r)}{k_s r} P_l(\cos \theta) \hat{\mathbf{r}} + \left[ h_{l-1}(k_s r) - \frac{h_l(k_s r)}{k_s r} \right] \frac{\partial P_l(\cos \theta)}{\partial \theta} \hat{\boldsymbol{\theta}} \right] \right\} \end{aligned} \quad (13)$$

Here  $h_k(x)$  are spherical Hankel functions of the second kind. Analytical expressions for the coefficients  $a_l$  and  $b_l$  are given in appendix B of Korneev and Johnson (1992), as well as information about the spherical vector system

$$\begin{aligned} \mathbf{Y}_{lm}^0 &\equiv \mathbf{Y}_{lm}^0(\theta, \phi) = \mathbf{r} \times \nabla Y_{lm}(\theta, \phi) \\ \mathbf{Y}_{lm}^+ &\equiv \mathbf{Y}_{lm}^+(\theta, \phi) = (l+1) \hat{\mathbf{r}} Y_{lm}(\theta, \phi) - r \nabla Y_{lm}(\theta, \phi) \\ \mathbf{Y}_{lm}^- &\equiv \mathbf{Y}_{lm}^-(\theta, \phi) = l \hat{\mathbf{r}} Y_{lm}(\theta, \phi) + r \nabla Y_{lm}(\theta, \phi) \end{aligned} \quad (14)$$

The definitions for the spherical harmonic functions are the usual ones

$$Y_{lm}(\theta, \phi) = e^{im\phi} P_l^m(\cos \theta) \quad , \quad l \geq 0 \quad , \quad (-l \leq m \leq l)$$

Any cylindrically symmetric scattered field (as we have for the case of an incident plane P wave) can be represented in the form of equation (13), where the coefficients  $a_l$  correspond to the compressional field and the coefficients  $b_l$  correspond to the shear field.

For the purpose of comparing different solutions, we will use the normalized scattering cross section  $\sigma_N$ , which is the ratio of the flow of the total energy carried outward by the scattered waves to the rate of flow in the incident wave through a normal area equal to the cross-sectional area of the object (geometric shadow of the object). In our case this is

$$\begin{aligned} \sigma_N &= \text{Im} \int_{r=r_0} \frac{(\mathbf{U}_2 \cdot \mathbf{t}_r^*[\mathbf{U}_2])}{\omega \alpha_2 (\lambda_2 + 2\mu_2) \pi R^2} ds = \sigma_N^{(p)} + \sigma_N^{(s)} \\ &= 4 \sum_{l \geq 0} (2l+1) \left\{ \left| \frac{a_l}{k_p R} \right|^2 + l(l+1) \gamma_2 \left| \frac{b_l}{k_s R} \right|^2 \right\} \end{aligned} \quad (15)$$

where  $\mathbf{t}_r[\mathbf{U}_2]$  is the stress vector of the field  $\mathbf{U}_2$  on the spherical surface of radius  $r_0$ , ( $r_0 > R$ ). The two parts of the scattering cross section,  $\sigma_N^{(p)}$  and  $\sigma_N^{(s)}$ , represent the P and S fields, respectively. It can be shown that the normalized scattered cross section  $\sigma_N$  is simply related to the forward scattered wave in the far field ( $r \rightarrow \infty$ )

$$\mathbf{U}_2(r, 0) \approx \frac{e^{-ik_p r}}{r} A_0 \hat{\mathbf{r}} = i \frac{e^{-ik_p r}}{k_p r} \sum_{l \geq 0} (2l+1) a_l \hat{\mathbf{r}}$$

through the formula

$$\sigma_N = -4 \frac{\text{Im} A_0}{k_p R^2} \quad (16)$$

This is the elastodynamic equivalent of an optical theorem.

#### 4. Low frequency solution for an elastic sphere of arbitrary contrast

Starting with the exact solution described in the previous section, it is possible to develop approximate solutions which are more general than the standard approximations given in section 2. First consider a low frequency approximation but with no restrictions upon the contrast in material properties. In this case we retain from the solution in equation (13) only the terms that are of lowest degree in frequency, which is  $\omega^3$  and appears only in the first three ( $l=0,1,2$ ) coefficients

$$\begin{aligned} a_0 &= i \frac{\xi^3}{6} \frac{\frac{3}{2}(\lambda_1 - \lambda_2) + \mu_1 - \mu_2}{\frac{1}{2}(\frac{3}{2}\lambda_1 + \mu_1) + \mu_2} \\ a_1 &= -i \frac{\xi^3}{9} \left[ \frac{\rho_1}{\rho_2} - 1 \right], \quad b_1 = i \frac{\eta^3}{9} \left[ \frac{\rho_1}{\rho_2} - 1 \right] \\ a_2 &= i \xi^3 \frac{4}{45} \left[ \frac{\mu_1}{\mu_2} - 1 \right] \frac{\gamma^2}{D}, \quad b_2 = -i \eta^3 \frac{2}{45} \left[ \frac{\mu_1}{\mu_2} - 1 \right] \frac{\gamma}{D} \end{aligned} \quad (17)$$

where

$$\begin{aligned} \xi &= k_p R, \quad \eta = k_s R \\ \gamma &= \frac{V_{s_1}}{V_{p_1}} \equiv \frac{V_s}{V_p}, \quad D = 1 + \frac{2}{15} \left[ \frac{\mu_1}{\mu_2} - 1 \right] (3 + 2\gamma^2) \end{aligned} \quad (18)$$

Then the solution has the form

$$\begin{aligned} \mathbf{U}_p &= \left[ \mathbf{U}_p \right]_r \hat{\mathbf{r}} + \left[ \mathbf{U}_p \right]_\theta \hat{\boldsymbol{\theta}} \\ &= A \left\{ \left[ -\frac{1}{2} \frac{\frac{3}{2}(\lambda_1 - \lambda_2) + \mu_1 - \mu_2}{\frac{1}{2}(\frac{3}{2}\lambda_1 + \mu_1) + \mu_2} W_{1r}^p(Z_p) + \left[ \frac{\rho_1}{\rho_2} - 1 \right] W_{1r}^p(Z_p) \cos\theta + \frac{2}{3} \left[ \frac{\mu_1}{\mu_2} - 1 \right] \frac{\gamma^2}{D} W_{2r}^p(Z_p) (1 - 3\cos^2\theta) \right] \hat{\mathbf{r}} \right. \\ &\quad \left. - \left[ \left[ \frac{\rho_1}{\rho_2} - 1 \right] W_{1\theta}^p(Z_p) \sin\theta - 2 \left[ \frac{\mu_1}{\mu_2} - 1 \right] \frac{\gamma^2}{D} W_{2\theta}^p(Z_p) \sin 2\theta \right] \hat{\boldsymbol{\theta}} \right\} \\ \mathbf{U}_s &= \left[ \mathbf{U}_s(\theta) \right]_r \hat{\mathbf{r}} + \left[ \mathbf{U}_s(\theta) \right]_\theta \hat{\boldsymbol{\theta}} \\ &= B \left\{ \left[ 2 \left[ \frac{\rho_1}{\rho_2} - 1 \right] W_{1r}^s(Z_s) \cos\theta + 2 \left[ \frac{\mu_1}{\mu_2} - 1 \right] \frac{\gamma}{D} W_{2r}^s(Z_s) (3\cos^2\theta - 1) \right] \hat{\mathbf{r}} \right. \end{aligned} \quad (19a)$$

$$+ \left[ - \left[ \frac{\rho_1}{\rho_2} - 1 \right] W_{1\theta}^i(Z_s) \sin\theta + \left[ \frac{\mu_1}{\mu_2} - 1 \right] \frac{\gamma}{D} W_{2\theta}^s(Z_s) \sin 2\theta \right] \hat{\theta} \} \quad (19b)$$

where the following functions have been introduced.

$$\begin{aligned} W_{0r}^p(Z_p) &= 1 - \frac{i}{Z_p} \\ W_{1r}^p(Z_p) &= 1 - 2 \frac{1 + iZ_p}{Z_p^2} , \quad W_{2r}^p(Z_p) = 1 + \frac{9i - 4iZ_p^2 - 9Z_p}{Z_p^3} \\ W_{1\theta}^s(Z_s) &= 1 - \frac{1 + iZ_s}{Z_s^2} , \quad W_{2\theta}^s(Z_s) = 1 + 3 \frac{2i - iZ_s^2 - 2Z_s}{Z_s^3} \\ W_{1\theta}^p(Z_p) &= \frac{1 + iZ_p}{Z_p^2} , \quad W_{2\theta}^p(Z_p) = \frac{3i - iZ_p^2 - 3Z_p}{Z_p^3} \\ W_{1r}^s(Z_s) &= \frac{1 + iZ_s}{Z_s^2} , \quad W_{2r}^s(Z_s) = \frac{3i - iZ_s^2 - 3Z_s}{Z_s^3} \end{aligned} \quad (20)$$

These  $W$  functions depend upon frequency  $\omega$  and radius  $r$  of the observation point through the parameters

$$Z_p = k_p r = \frac{\omega r}{V_p} , \quad Z_s = k_s r = \frac{\omega r}{V_s}$$

The expression in equation (19) is a complete low frequency solution in that it contains both the near field and far field parts. All of the distance dependence in the solution is contained in the  $W$  functions of equation (20). We obtain the far field asymptotic form of the solution if the functions in equation (20) satisfy the following conditions

$$\left| W_{0r}^p(Z_p) \right| \approx 1 , \quad \left| W_{1r}^p(Z_p) \right| \approx 1 , \quad \left| W_{2r}^p(Z_p) \right| \approx 1 , \quad \left| W_{1\theta}^s(Z_s) \right| \approx 1 , \quad \left| W_{2\theta}^s(Z_s) \right| \approx 1 \quad (21a)$$

$$\left| W_{1\theta}^p(Z_p) \right| \approx 0 , \quad \left| W_{2\theta}^p(Z_p) \right| \approx 0 , \quad \left| W_{1r}^s(Z_s) \right| \approx 0 , \quad \left| W_{2r}^s(Z_s) \right| \approx 0 \quad (21b)$$

The functions in equation (20) are graphed in Figure 1 for the case of  $\gamma = V_s/V_p = Z_p/Z_s = 1/\sqrt{3}$ . This figure shows that for  $k_p r < 1$  the far field approximation is definitely not satisfied. As  $\omega$  increases the situation improves and for  $k_p r > 3$  equation (21a) is satisfied to within 10%. However, the terms of equation (21b) converge to their asymptotic values much more slowly and, while three of these terms have converged to within 10% of zero for  $k_p r > 10$ , the  $W_{2\theta}^p$  term does not decrease to this level until  $k_p r > 20$ .

What this means is that at observation distances  $r$  that are only a few times greater than the wavelength the amplitudes of the scattered waves may be consistent with the far field approximation but their polarizations will be considerably more complicated than simple P and S waves.

The situation is slightly more complicated than indicated in Figure 1. In that figure the absolute values of the W functions are plotted, but in equation (19) it is clear that these functions can combine either constructively or destructively, depending upon the difference in material properties and the azimuth of the observation point. Furthermore, at small distances and low frequencies it can be misleading to consider the individual terms of the solution, as what appears to be a large individual term may be canceled out by another and not show up in the total solution. Thus in Figure 2 the effect of the near field terms in the scattered field is illustrated by showing the complete solutions in the time domain. Here the P wave scattered from a homogeneous spherical inclusion is shown at one azimuth and a distance that is 6 times the radius of the inclusion, which corresponds to  $k_p r = 1.2$ . The near field terms make a significant contribution at this distance, affecting both the amplitude and the polarization of the scattered wave.

In the true far field where all of the conditions of equation (21) are satisfied, the scattered field has the form

$$U_p = A \left\{ -\frac{1}{2} \frac{\frac{3}{2}(\lambda_1 - \lambda_2) + \mu_1 - \mu_2}{\frac{1}{2}(\frac{3}{2}\lambda_1 + \mu_1) + \mu_2} + \left[ \frac{\rho_1}{\rho_2} - 1 \right] \cos\theta + \frac{2}{3} \left[ \frac{\mu_1}{\mu_2} - 1 \right] \frac{\gamma^2}{D} (1 - 3\cos^2\theta) \right\} \hat{r} \quad (22a)$$

$$U_s = B \left\{ -\left[ \frac{\rho_1}{\rho_2} - 1 \right] \sin\theta + \left[ \frac{\mu_1}{\mu_2} - 1 \right] \frac{\gamma}{D} \sin 2\theta \right\} \hat{\theta} \quad (22b)$$

This result represents Rayleigh scattering from an obstacle having an arbitrary contrast in material properties. In the case where the contrast is small and the conditions of equation (3) are satisfied, then equation (22) reduces to (6) and we have the combined approximations of low frequency, far field, and low contrast. Thus in the progression of solutions in equations (13), (19), (22), and (6) we see the effects of the Rayleigh and Born approximations.

The Mie scattering solution for a homogeneous sphere in equation (11) can be easily generalized to an sphere of arbitrary contrast to obtain

$$\mathbf{U}_p = A \left\{ -\frac{1}{2} \frac{\frac{3}{2}(\lambda_1 - \lambda_2) + \mu_1 - \mu_2}{\frac{1}{2}(\frac{3}{2}\lambda_1 + \mu_1) + \mu_2} + \left[ \frac{\rho_1}{\rho_2} - 1 \right] \cos\theta + \frac{2}{3} \left[ \frac{\mu_1}{\mu_2} - 1 \right] \frac{\gamma^2}{D} (1 - 3\cos^2\theta) \right\} \frac{j_1(q_1)}{q_1} \hat{\mathbf{r}} \quad (23a)$$

$$\mathbf{U}_s = B \left\{ -\left[ \frac{\rho_1}{\rho_2} - 1 \right] \sin\theta + \left[ \frac{\mu_1}{\mu_2} - 1 \right] \frac{\gamma}{D} \sin 2\theta \right\} \frac{j_1(q_2)}{q_2} \hat{\boldsymbol{\theta}} \quad (23b)$$

In order to compare the various approximations discussed above, the normalized cross sections of equation (15) are plotted as a function of  $k_p R$  in Figure 3. Such results are shown for two different cases, a low velocity inclusion on the top and a high velocity inclusion on the bottom. The contrast in the velocities and densities is about 20%. The four solutions shown in this figure are the exact of equation (13), the Born-Rayleigh approximation of equation (6), the arbitrary contrast Rayleigh of equation (22), and the arbitrary contrast Mie of equation (23). Note that the far field approximation has been made in all of these solutions. In order to calculate scattering cross sections from the solution in equation (23) it was necessary to convert this solution to the form of equation (13) using the orthogonal properties of the spherical vectors in equation (14), and then substitute the obtained coefficients  $a_l$  and  $b_l$  into equation (15). It should be pointed out that scattering cross sections for the case of Rayleigh scattering from a spherical inclusion of arbitrary contrast were also obtained by Ying and Truell (1956) using potential functions.

The results shown in Figure 3 help define the frequency ranges over which the various approximations are valid. First note that the Born-Rayleigh approximation is the least accurate of those shown in this figure and that the sign of the error is different for low-velocity and high-velocity inclusions. For the case of the low-velocity inclusion this approximation falls below the exact solution at low frequencies and the error reaches appreciable values in the range around  $k_p R = 0.4$ , whereas in the case of the high-velocity inclusion the approximate solution falls above the exact solution and the error exceeds 100% for  $k_p R > 0.3$ . In contrast to this, the arbitrary contrast Rayleigh approximation behaves about the same for the low-velocity and high-velocity inclusions and remains reasonably accurate for  $k_p R < 0.5$ . A result which is very clear in this figure is that by far the best approximation to the exact solution is provided by the arbitrary contrast Mie solution. This approximation is reasonably valid for  $k_p R < 6$  for the low velocity inclusion and for  $k_p R < 4$  for the high velocity inclusion, which is an order of magnitude broader range than for the other approximations. Of course, these ranges of validity will vary somewhat with the values of the

material properties which are used, but our calculations indicate that the results shown in Figure 3 display the primary features present in the general case.

### 5. Low contrast approximation

Another type of approximate solution which can be derived from the exact solution of section 3 is one which assumes a small contrast in material properties between the inclusion and surrounding media, but places fewer restrictions upon the applicable frequency range than does the Rayleigh approximation. For the case in equation (3) of small perturbations in the elastic parameters of the inclusion, the coefficients  $a_l$  and  $b_l$  of equation (13) (the original expressions can be found in Appendix B of Korneev and Johnson, 1992) can be reduced to the following expressions

$$a_l = i\xi^3 \left\{ \frac{1}{2} \frac{\delta\lambda + 2\delta\mu}{\lambda + 2\mu} \left[ j_l^2(\xi) - j_{l+1}(\xi)j_{l-1}(\xi) \right] + \frac{\delta\mu}{\lambda + 2\mu} \frac{2}{\xi^2} \left[ l(l-1) \frac{j_l(\xi)}{\xi} (j_{l-1}(\xi) - j_{l+1}(\xi)) - 2j_{l+1}^2(\xi) \right] \right. \\ \left. - \frac{1}{2} \frac{\delta\rho}{\rho} \left[ j_l^2(\xi) + j_{l+1}^2(\xi) - (2l+3) \frac{j_l(\xi)}{\xi} j_{l+1}(\xi) + 2l \frac{j_l^2(\xi)}{\xi^2} \right] \right\} \quad (24a)$$

$$b_l = i\eta^3 \left\{ \frac{\delta\mu}{\lambda + 2\mu} \frac{2}{\xi^2} \left[ j_{l+1}(\eta) \left( (l-1) \frac{j_l(\xi)}{\xi} - j_{l+1}(\xi) \right) - (l-1) \frac{j_l(\eta)}{\eta} j_{l-1}(\xi) \right] + \frac{\delta\rho}{\rho} \frac{j_l(\eta)}{\eta} \frac{j_l(\xi)}{\xi} \right\} \quad (24b)$$

These solutions are not completely general in frequency, because the manipulations of the Bessel functions that were used in obtaining them are only strictly valid when we have

$$\xi_1 - \xi_2 \approx k_p R \frac{1}{2} \left[ \frac{\delta\lambda + 2\delta\mu}{\lambda + 2\mu} - \frac{\delta\rho}{\rho} \right] < \frac{\pi}{10}, \quad \eta_1 - \eta_2 \approx k_s R \frac{1}{2} \left[ \frac{\mu}{\mu} - \frac{\delta\rho}{\rho} \right] < \frac{\pi}{10} \quad (25)$$

This restriction places an upper limit upon the valid frequency range for equation (24), with this limit increasing as the contrast in material properties becomes smaller and smaller. Below we will show that this restriction is significant for the  $a_l$  coefficients but not for the  $b_l$  coefficients.

Given that the low contrast solution of equation (24) is most appropriate for low frequencies that satisfy the restriction of equation (25), we can proceed differently to obtain solutions that are more appropriate for the higher frequencies. Here we follow the method described by Van der Hulst (1957) for the scattering of light from large low contrast spheres. The basic procedure is to substitute Debye



asymptotic expansions for the Bessel functions into the exact analytical expressions. Starting with the exact analytical expressions for the coefficients of equation (13), the low contrast assumption is made and then it is possible to obtain the following approximate expression for the coefficients of the scattered P wave.

$$a_l = - \frac{j_{l+1}(\xi_1) j_l(\xi_2) - \kappa j_l(\xi_1) j_{l+1}(\xi_2)}{j_{l+1}(\xi_1) h_l(\xi_2) - \kappa j_l(\xi_1) h_{l+1}(\xi_2)} \quad (26)$$

where

$$\kappa = \frac{\rho_1}{\rho_2} \frac{V_{p1}}{V_{p2}}$$

Then we write equation (26) in the form

$$a_l = - \frac{\tan(\alpha_l)}{\tan(\alpha_l) - i} = -\frac{1}{2} \left[ 1 - e^{-2i\alpha_l} \right] \quad (27)$$

where

$$\tan(\alpha_l) = - \frac{j_{l+1}(\xi_1) j_l(\xi_2) - \kappa j_l(\xi_1) j_{l+1}(\xi_2)}{j_{l+1}(\xi_1) n_l(\xi_2) - \kappa j_l(\xi_1) n_{l+1}(\xi_2)}$$

and the  $n_l(\xi)$  are spherical Neuman functions. Because we are looking for solutions valid at high frequencies, we introduce the Debye asymptotic expansions

$$j_l(\xi) = \frac{\cos(\xi f - \frac{\pi}{4})}{\xi \sqrt{\tau}}$$

$$n_l(\xi) = - \frac{\sin(\xi f - \frac{\pi}{4})}{\xi \sqrt{\tau}}$$

where

$$f = \sin \tau - \tau \cos \tau, \text{ and } \cos \tau = \frac{l + \frac{1}{2}}{\xi}$$

These approximations are valid for  $l + \frac{1}{2} < \xi$ . Now equation (27) can be reduced to

$$a_l = -\frac{1}{2} \left[ 1 - e^{2i(\xi_1 f_1 - \xi_2 f_2)} \frac{1 - ike^{2i\xi_1 f_1}}{1 + ike^{-2i\xi_1 f_1}} \right] \quad (28)$$

where

$$k = \frac{\kappa - 1}{\kappa + 1}$$

If the low contrast conditions of equation (3) are strongly satisfied, equation (28) can be further simplified to yield

$$a_l = -\frac{1}{2} \left[ 1 - e^{-ia} \right] \quad (29)$$

where

$$a = 2 \left[ 1 - \frac{V_{p1}}{V_{p2}} \right] \xi \quad (30)$$

This is identical to the solution that is obtained in optics. Substituting the  $a_l$  of equation (29) into the optical theorem of equation (16) results in a simple formula for the normalized scattering cross section (Morozhnik, 1983).

$$\sigma_N \approx \sigma_N^{(p)} = 2 - \frac{4}{a} \sin a + \frac{4}{a^2} (1 - \cos a) \quad (31)$$

An earlier derivation of equation (31) can be found in Van der Hulst (1957), where it is shown that this result can be explained by interference of the incident and refracted waves propagating in the forward direction. The parameter  $a$  is just the phase difference between these two waves in the far field.

Two different formulas have been developed above for the coefficients of the scattered P waves in the low contrast case. At frequencies low enough so that equation (25) is satisfied, equation (24a) should be used. At higher frequencies equation (28) should be used, and when the low contrast assumption is strongly satisfied this can be replaced by equation (29). The high frequency solution is valid so long as  $\xi \leq l + \frac{1}{2}$ . The relationship between these different approximate solutions for the scattered P wave is illustrated in Figure 4 for two different cases, a low velocity inclusion and a high velocity inclusion. In both cases the contrast in velocities and densities is about 5%. This figure shows the scattering cross section of the exact solution for the scattered P field of equation (13) and for two approximate solutions, the low-frequency P field of equation (24) and the high-frequency P field of equation (28). Also shown is the

scattering cross section which is calculated using the analytical expression of equation (31). At low frequencies the approximate solution of equation (24a) agrees best with the exact solution for the scattered P field, with the error growing to about 30% by the time that the condition of equation (25) is exceeded ( $k_p R \approx 3$ ). The high frequency approximate solution in equation (28) as well as equation (31) both systematically over estimate the exact solution in this range. At higher frequencies the situation is reversed. The low frequency approximate solution of equation (24a) tracks the exact solution reasonably well up to about  $k_p R \approx 5$  and then is completely wrong at higher frequencies. The high frequency approximate solution of equation (28) and equation (31) agree quite well with the exact solution for  $k_p R \geq 5$ , showing the same oscillatory behavior at a slightly reduced amplitude for the low-velocity inclusion and at a slightly increased amplitude for the high-velocity inclusion. In this range these two approximate results are so close to each other that they appear as one line on the graph. This demonstrates that the very simple analytical expression of equation (31) provides an excellent approximation to the scattering cross section for the high-frequency low-contrast case.

For the scattered S waves in the low contrast approximation we return to equation (24b) for the  $b_l$  coefficients. In this case the condition of equation (25) does not restrict the use of equation (24b) because the higher order  $b_l$  coefficients decrease sufficiently rapidly with increasing frequency. At high frequencies the S part of the scattering cross-section,  $\sigma_N^{(s)}$ , oscillates slightly about a constant level. Substituting equation (24b) into equation (15) for  $\sigma_N^{(s)}$  and numerically evaluating the infinite sum of the products of Bessel functions, we obtain the high-frequency asymptotic estimate

$$\begin{aligned} \sigma_N^{(s)} &= 4 \sum_{l=0}^{\infty} l(l+1)(2l+1) \gamma \left| \frac{b_l}{\eta} \right|^2 \\ &\approx 4.2 \gamma^4 \frac{\delta \mu^2}{\mu^2} - 6.0 \gamma^4 \frac{V_{s1}^2}{V_{s2}^2} \frac{\delta \mu}{\mu} \frac{\delta \rho}{\rho} + 1.8 \gamma^4 \frac{\delta \rho^2}{\rho^2} \end{aligned} \quad (32)$$

Thus we see that in the limit of large frequency, the scattering cross section of the S waves reduces to a constant independent of frequency.

An example of the various solutions for the normalized scattering cross sections for the S field is shown in Figure 5. It is clear that the low contrast solution calculated from equation (24b) is a good

approximation to the exact solution for both cases of a low-velocity inclusion and a high-velocity inclusion. The agreement is extremely good for  $k_p R < 1$ , but even at higher frequencies the approximate result tracks the main features of the exact result and never differs from it by more than about 25%. Similar to the scattered P field, this approximate solution under estimates the exact solution in the case of a low-velocity inclusion and over estimates it in the case of a high-velocity inclusion. Also shown on this plot is the high frequency asymptotic approximation of equation (32). While this is obviously not an appropriate approximation at the very low frequencies, it provides a simple but fairly accurate result at higher frequencies. It is worth noting that the examples shown in Figures 4 and 5 actually represent a severe test for the low-contrast approximations. While the contrasts in velocities and densities are only 5% in these examples, the contrasts in elastic constants are about 15%.

Also shown in Figure 5 for the purposes of comparison is the exact solution for the normalized scattering cross section of the P field. The scattered P field is clearly much larger than the scattered S field for high frequencies, but for  $k_p R < 1$  the situation can be reversed, with the scattered S field considerably larger than the scattered P field. To a certain degree this type of behavior is a function of the contrasts in material properties of the inclusion, but there is generally a range of frequencies where more energy is scattered into the S field than into the P field. This observation could have implications for the generation of seismic coda.

## 6. Conclusions

There are two basic lessons to be learned from this study. First, considerable care must be taken in using various approximate solutions for the seismic scattering problem because these solutions are valid only over a limited range of conditions. Second, standard approximations that are typically made in seismology and associated with the names of Born, Rayleigh, and Mie can be considerably improved by making a few modifications in the formulae or by using some of the alternative formulae developed in this study. Because of the need to make comparisons with exact solutions, this study has concentrated on the case of P waves scattered from a spherical inclusion. However, the results are more general than this and should be applicable to scattering from a more extended class of objects with simple and smooth

boundaries.

The Born-Rayleigh approximation is commonly made in seismology for the case of low contrast scatterers and wavelengths large compared to the dimensions of the scatterer. However, because of the effect of near field terms in the scattering solution, this approximation is only valid at distances which are removed several wavelengths from the site of the scattering. Thus care must be taken in using this type of an approximation to explain scattering in the vicinity of seismographic stations.

Both the usual Rayleigh approximation of equation (6) and the Mie approximation of equation (10) are limited to low frequencies and low contrasts in material properties. The low contrast limitation can be considerably expanded by using solutions developed as a low frequency approximation for an inclusion of arbitrary contrast. Thus, by substituting equation (22) for the Rayleigh formula of equation (6) and by substituting equation (23) for the Mie formula of equation (11) the range of validity of these solutions can be extended to higher frequencies. In particular, as shown in Figure 3, the arbitrary contrast Mie solution is valid over a frequency range that is an order of magnitude greater than for the other approximate solutions.

In situations where the contrast in material properties is actually small, approximate solutions have been developed that are valid over essentially the entire frequency range. In the case of an incident P wave two different results must be used for the scattered P field, one for the low frequencies and one for the high frequencies. However, a single result can be used for the scattered S field over the entire frequency range. For situations where the scattering cross section is needed, an analytical result based on the optical theorem provides a simple but good approximation for the higher frequencies. Finally, these results illustrate some of the important differences between acoustic and elastic scattering, as there are frequencies where considerably more energy is scattered into S waves than into P waves.

#### **Acknowledgments**

This research was supported by Phillips Laboratory under Contract F19628-90- K-0055 and also by the U.S. Department of Energy under Contract DE- AC03-76SF00098.

## References

- Aki, K. and Chouet B., 1975. Origin of coda-waves : source, attenuation and scattering effects, *J. Geophys. Res.*, **80**, 3322-3342.
- Chernov, L. A., 1960. *Wave Propagation in a Random Medium*, English transl., Dover, New York, 168 pp.
- Hudson, J. A. and Heritage, J. R., 1981. The use of the Born approximation in the seismic scattering problem, *Geophys. J. R. Astron. Soc.*, **66**, 221-240.
- Korneev, V. A., and Johnson, L. R., 1992. Scattering of elastic waves by a spherical inclusion - 1. Theory and numerical results, submitted.
- Morochnik, V. S., 1983. Scattering of compressional elastic waves by a low-contrast spherical inclusion, *Izvestia Acad. Nauk USSR, Fizika Zemli* **7**, 65-72.
- Sato, H., 1984. Attenuation and envelope formation of three- component seismograms of small local earthquakes in randomly inhomogeneous lithosphere, *J. Geophys. Res.*, **89**, 1221-1241.
- Van der Hulst, H. C., 1957. *Light Scattering by Small Particles*, John Wiley and Sons, New York, 470 pp.
- Wu, R. and Aki, K., 1985a. Scattering characteristics of elastic waves by an elastic heterogeneity, *Geophysics*, **50**, 582-595.
- Wu R. and Aki K. , 1985b. Elastic wave scattering by a random medium and the small-scale inhomogeneities in the lithosphere, *J. of Geophys. Res.*, **90**, 10,261-10,273.
- Ying, C. F., and Truell, R., 1956. Scattering of a plane longitudinal wave by a spherical obstacle in an isotropically elastic solid, *J. Appl. Physics*, **27**, 1086-1097.

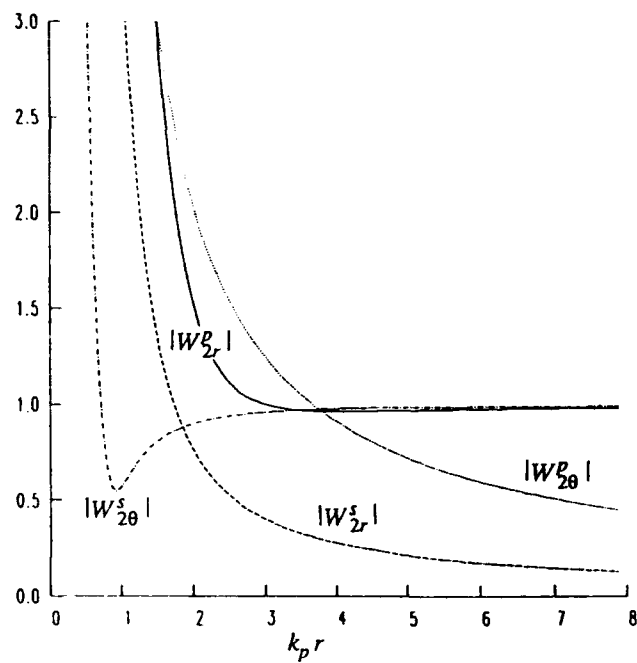
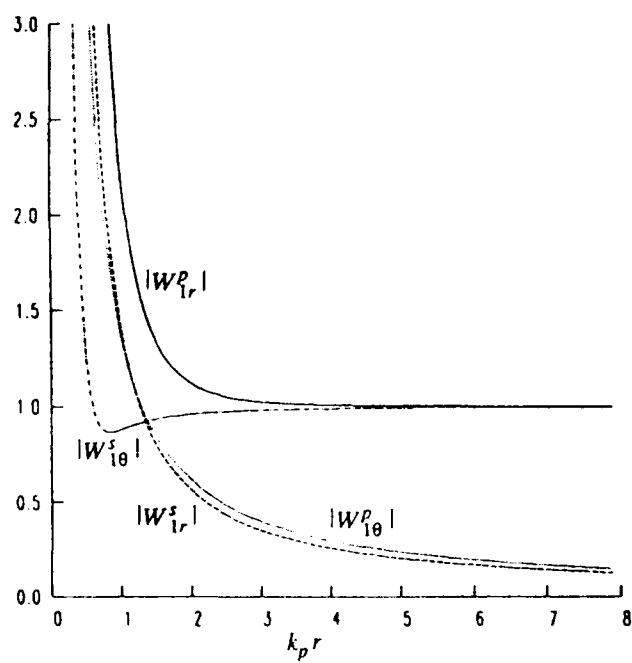
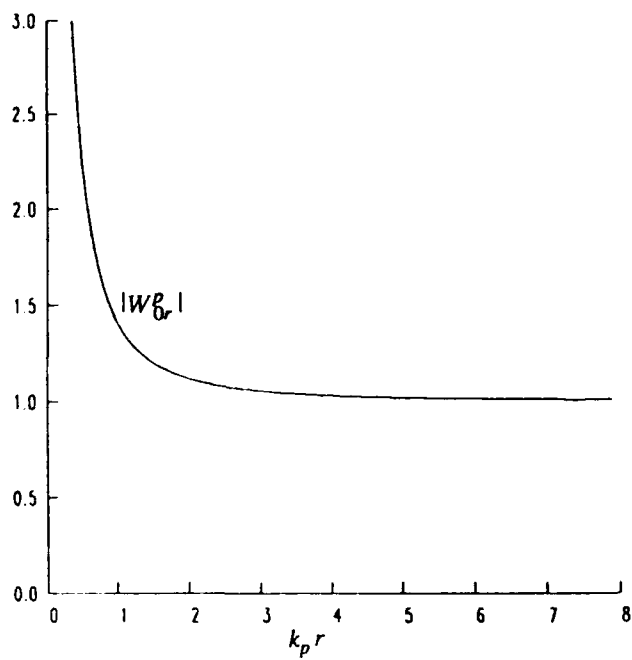


**Figure 1.** Moduli of the  $W$  functions which control the distance dependence of the scattered fields in the low frequency approximation.

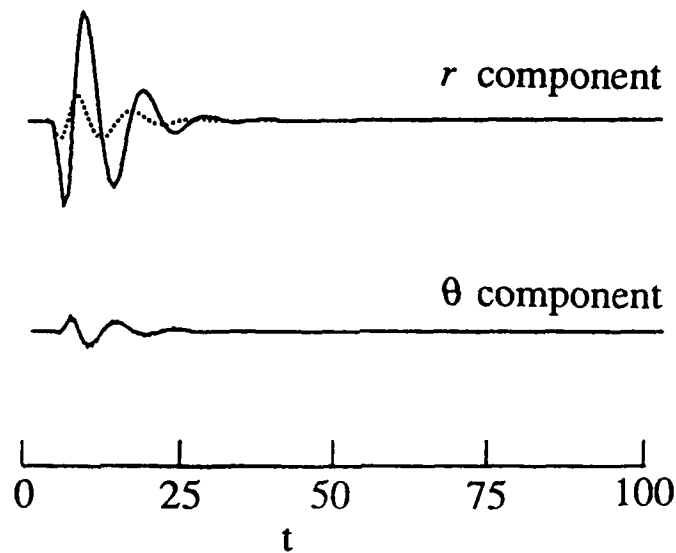


**Figure 2.** Synthetic seismograms that show the effects of near field terms in the scattered fields. A plane P wave is incident upon a high-velocity sphere for which  $V_p/V_{p1} = V_s/V_{s1} = 1.25$  and  $\rho_1/\rho_2 = 1.10$ . The dominant angular frequency of the input pulse is  $\omega = 0.2 V_p/R$ , where  $R$  is the radius of the sphere. The seismograms are calculated at a radial distance  $r = 6R$  and an azimuth  $\theta = 45^\circ$ . The units of the time  $t$  are  $R/V_p$ . The solid line is the complete solution, whereas the dotted line includes only the far field parts of the solution.



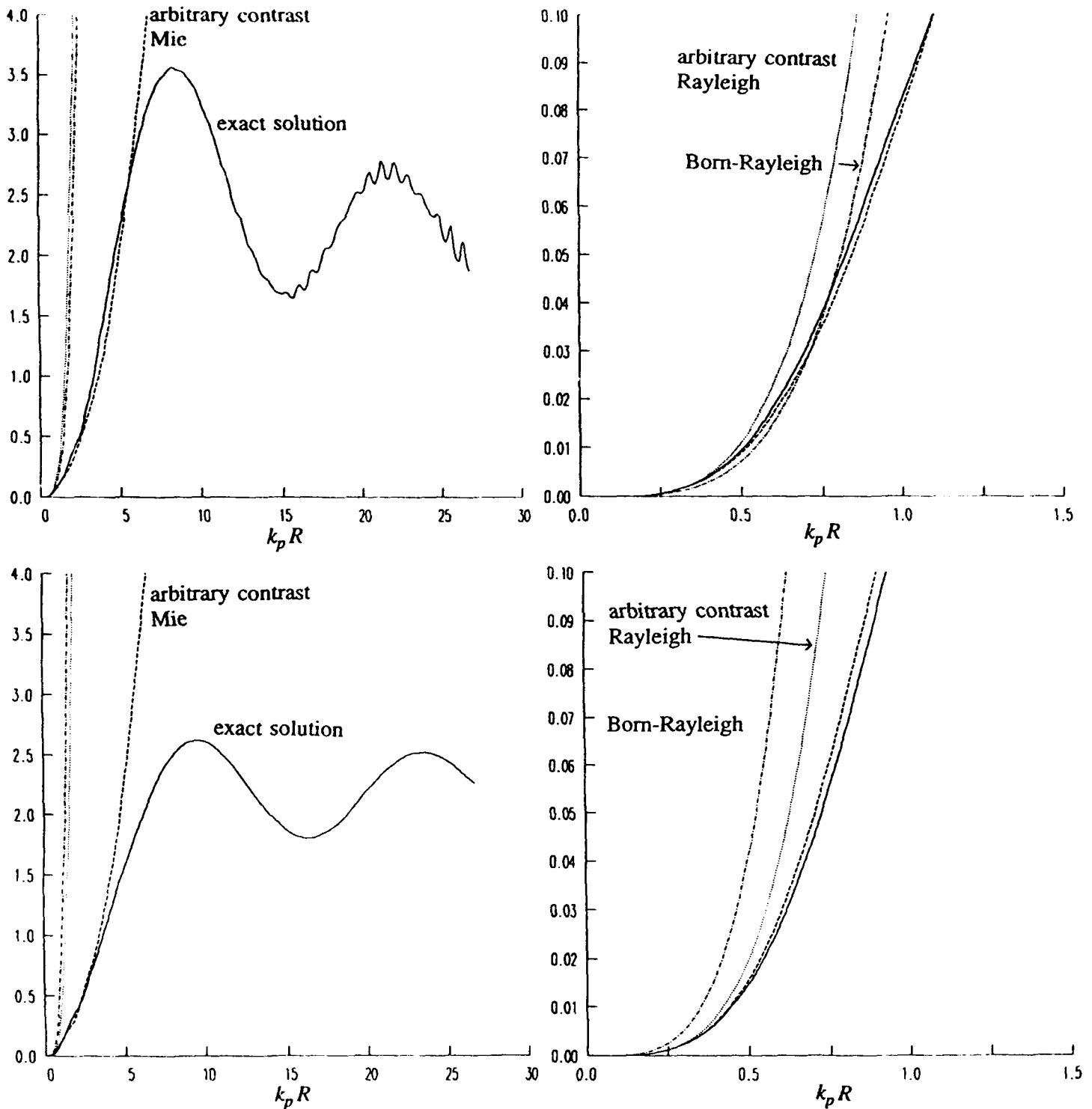


**Figure 3.** Normalized scattering cross sections as a function of frequency. The upper two panels are for a low velocity inclusion with  $V_p/V_{p1} = V_s/V_{s1} = 0.8$  and  $\rho_1/\rho_2 = 0.9$ , while the lower panels are for a high velocity inclusion with  $V_p/V_{p1} = V_s/V_{s1} = 1.3$  and  $\rho_1/\rho_2 = 1.2$ . The panels on the right are expanded versions of those on the left for small values of the arguments.

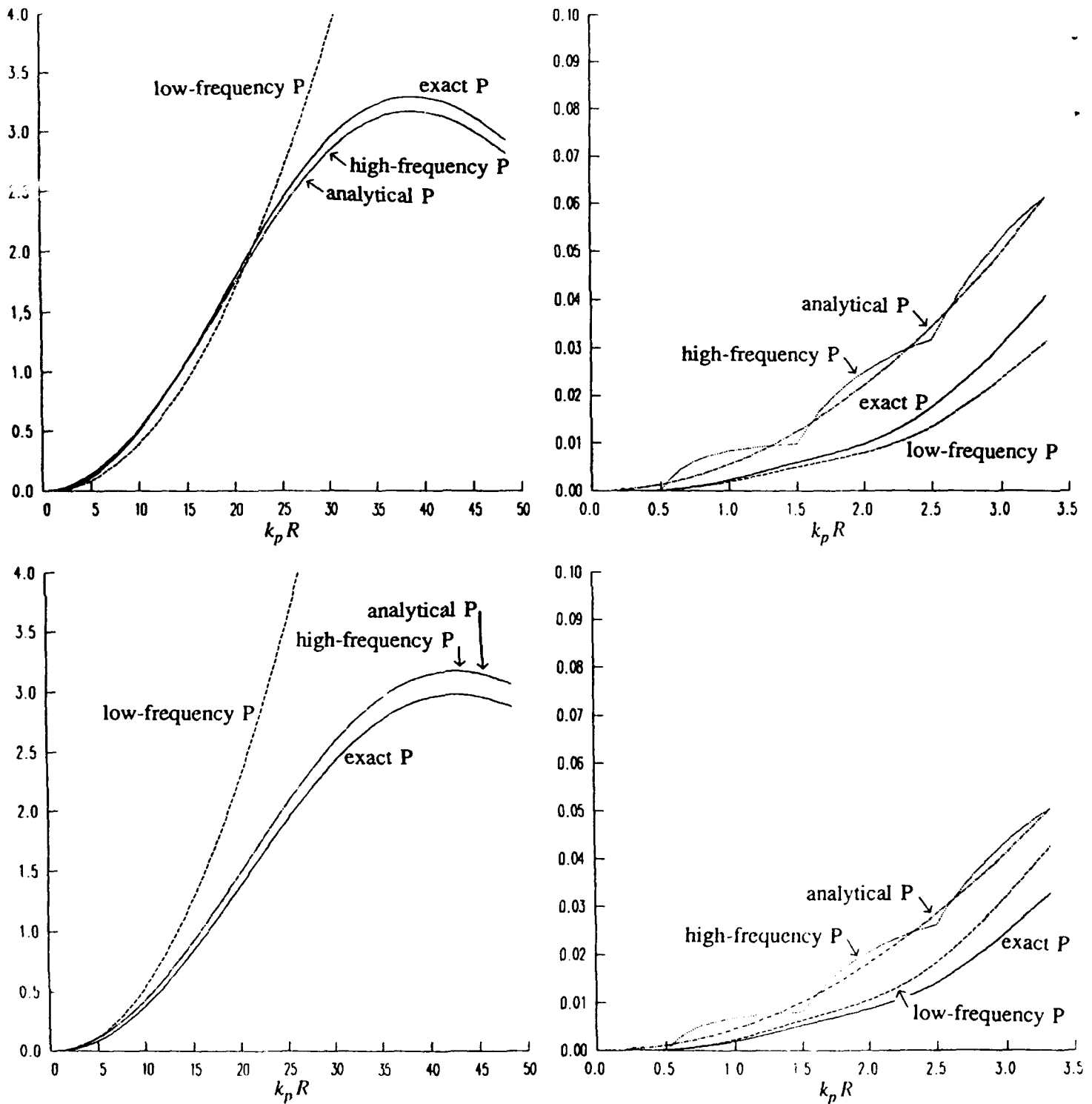


**Figure 4.** Normalized scattering cross sections as a function of frequency for the scattered P field in the low-contrast case. The upper two figures are for a low velocity inclusion with  $V_p/V_{p1} = V_s/V_{s1} = \rho_1/\rho_2 = 0.95$ , while the lower figures are for a high velocity inclusion with  $V_p/V_{p1} = V_s/V_{s1} = \rho_1/\rho_2 = 1.05$ . The panels on the right are expanded versions of those on the left for small values of the arguments.

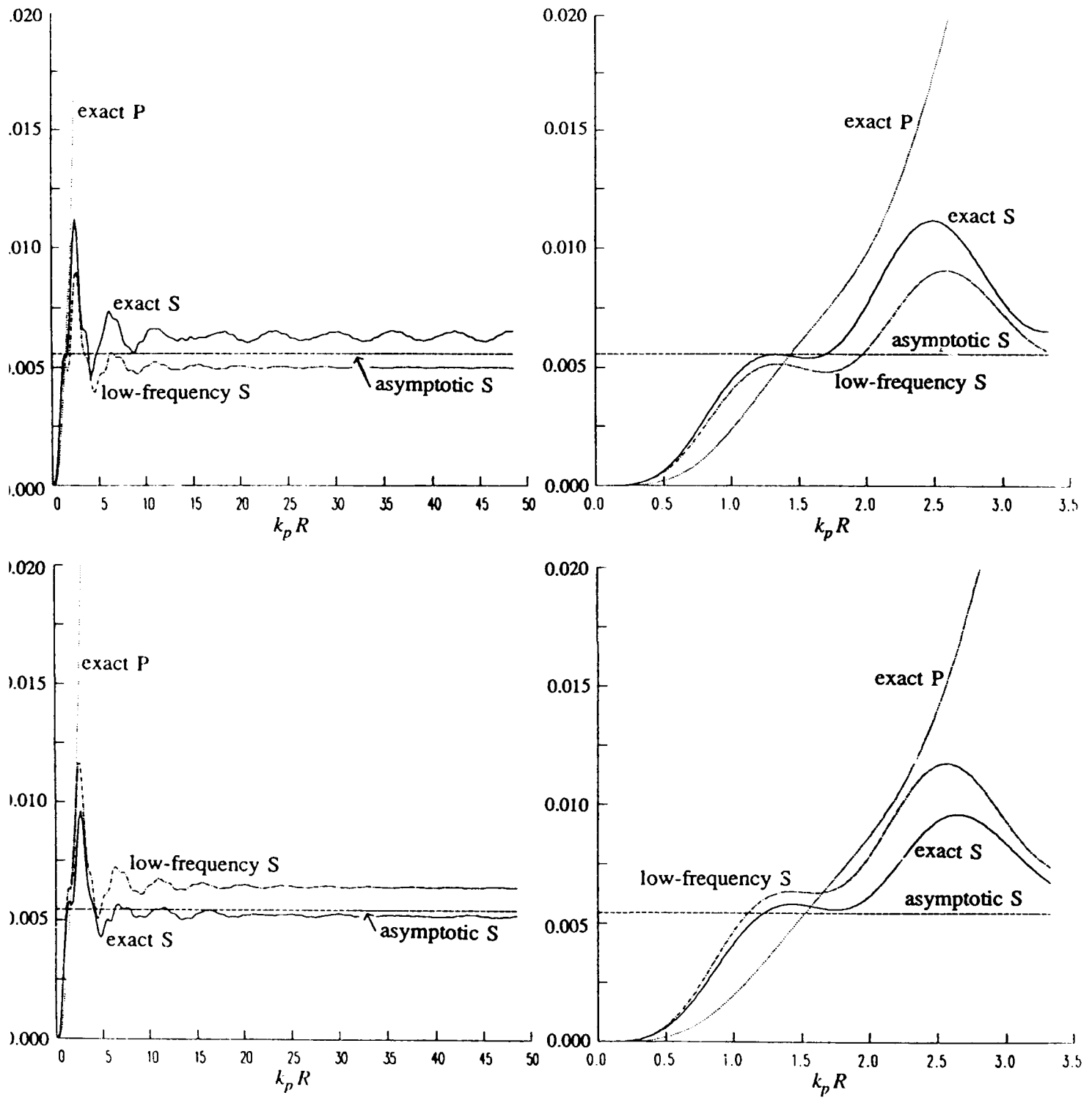


**Figure 5.** Similar to Figure 4 for the scattered S field. Also shown for comparison is the exact P field from Figure 4.

DISTRIBUTION LIST

Prof. Thomas Ahrens  
Seismological Lab, 252-21  
Division of Geological & Planetary Sciences  
California Institute of Technology  
Pasadena, CA 91125

Prof. Keiiti Aki  
Center for Earth Sciences  
University of Southern California  
University Park  
Los Angeles, CA 90089-0741

Prof. Shelton Alexander  
Geosciences Department  
403 Deike Building  
The Pennsylvania State University  
University Park, PA 16802

Dr. Ralph Alewine, III  
DARPA/NMRO  
3701 North Fairfax Drive  
Arlington, VA 22203-1714

Prof. Charles B. Archambeau  
CIRES  
University of Colorado  
Boulder, CO 80309

Dr. Thomas C. Bache, Jr.  
Science Applications Int'l Corp.  
10260 Campus Point Drive  
San Diego, CA 92121 (2 copies)

Prof. Muawia Barazangi  
Institute for the Study of the Continent  
Cornell University  
Ithaca, NY 14853

Dr. Jeff Barker  
Department of Geological Sciences  
State University of New York  
at Binghamton  
Vestal, NY 13901

Dr. Douglas R. Baumgardt  
ENSCO, Inc  
5400 Port Royal Road  
Springfield, VA 22151-2388

Dr. Susan Beck  
Department of Geosciences  
Building #77  
University of Arizona  
Tucson, AZ 85721

Dr. T.J. Bennett  
S-CUBED  
A Division of Maxwell Laboratories  
11800 Sunrise Valley Drive, Suite 1212  
Reston, VA 22091

Dr. Robert Blandford  
AFTAC/TT, Center for Seismic Studies  
1300 North 17th Street  
Suite 1450  
Arlington, VA 22209-2308

Dr. G.A. Bollinger  
Department of Geological Sciences  
Virginia Polytechnical Institute  
21044 Derring Hall  
Blacksburg, VA 24061

Dr. Stephen Bratt  
Center for Seismic Studies  
1300 North 17th Street  
Suite 1450  
Arlington, VA 22209-2308

Dr. Lawrence Burdick  
Woodward-Clyde Consultants  
566 El Dorado Street  
Pasadena, CA 91109-3245

Dr. Robert Burrige  
Schlumberger-Doll Research Center  
Old Quarry Road  
Ridgefield, CT 06877

Dr. Jerry Carter  
Center for Seismic Studies  
1300 North 17th Street  
Suite 1450  
Arlington, VA 22209-2308

Dr. Eric Chael  
Division 9241  
Sandia Laboratory  
Albuquerque, NM 87185

Prof. Vernon F. Cormier  
Department of Geology & Geophysics  
U-45, Room 207  
University of Connecticut  
Storrs, CT 06268

Prof. Steven Day  
Department of Geological Sciences  
San Diego State University  
San Diego, CA 92182

Marvin Denny  
U.S. Department of Energy  
Office of Arms Control  
Washington, DC 20585

Dr. Zoltan Der  
ENSCO, Inc.  
5400 Port Royal Road  
Springfield, VA 22151-2388

Prof. Adam Dziewonski  
Hoffman Laboratory, Harvard University  
Dept. of Earth Atmos. & Planetary Sciences  
20 Oxford Street  
Cambridge, MA 02138

Prof. John Ebel  
Department of Geology & Geophysics  
Boston College  
Chestnut Hill, MA 02167

Eric Fielding  
SNEE Hall  
INSTOC  
Cornell University  
Ithaca, NY 14853

Dr. Mark D. Fisk  
Mission Research Corporation  
735 State Street  
P.O. Drawer 719  
Santa Barbara, CA 93102

Prof Stanley Flatte  
Applied Sciences Building  
University of California, Santa Cruz  
Santa Cruz, CA 95064

Dr. John Foley  
NER-Geo Sciences  
1100 Crown Colony Drive  
Quincy, MA 02169

Prof. Donald Forsyth  
Department of Geological Sciences  
Brown University  
Providence, RI 02912

Dr. Art Frankel  
U.S. Geological Survey  
922 National Center  
Reston, VA 22092

Dr. Cliff Frolich  
Institute of Geophysics  
8701 North Mopac  
Austin, TX 78759

Dr. Holly Given  
IGPP, A-025  
Scripps Institute of Oceanography  
University of California, San Diego  
La Jolla, CA 92093

Dr. Jeffrey W. Given  
SAIC  
10260 Campus Point Drive  
San Diego, CA 92121

Dr. Dale Glover  
Defense Intelligence Agency  
ATTN: ODT-1B  
Washington, DC 20301

Dr. Indra Gupta  
Teledyne Geotech  
314 Montgomery Street  
Alexandria, VA 22314

Dan N. Hagedorn  
Pacific Northwest Laboratories  
Battelle Boulevard  
Richland, WA 99352

Dr. James Hannon  
Lawrence Livermore National Laboratory  
P.O. Box 808  
L-205  
Livermore, CA 94550

Dr. Roger Hansen  
HQ AFTAC/TTR  
Patrick AFB, FL 32925-6001

Prof. David G. Harkrider  
Seismological Laboratory  
Division of Geological & Planetary Sciences  
California Institute of Technology  
Pasadena, CA 91125

Prof. Danny Harvey  
CIRES  
University of Colorado  
Boulder, CO 80309

Prof. Donald V. Helmberger  
Seismological Laboratory  
Division of Geological & Planetary Sciences  
California Institute of Technology  
Pasadena, CA 91125

Prof. Eugene Herrin  
Institute for the Study of Earth and Man  
Geophysical Laboratory  
Southern Methodist University  
Dallas, TX 75275

Prof. Robert B. Herrmann  
Department of Earth & Atmospheric Sciences  
St. Louis University  
St. Louis, MO 63156

Prof. Lane R. Johnson  
Seismographic Station  
University of California  
Berkeley, CA 94720

Prof. Thomas H. Jordan  
Department of Earth, Atmospheric &  
Planetary Sciences  
Massachusetts Institute of Technology  
Cambridge, MA 02139

Prof. Alan Kafka  
Department of Geology & Geophysics  
Boston College  
Chestnut Hill, MA 02167

Robert C. Kemerait  
ENSCO, Inc.  
445 Pineda Court  
Melbourne, FL 32940

Dr. Max Koontz  
U.S. Dept. of Energy/DP 5  
Forrestal Building  
1000 Independence Avenue  
Washington, DC 20585

Dr. Richard LaCoss  
MIT Lincoln Laboratory, M-200B  
P.O. Box 73  
Lexington, MA 02173-0073

Dr. Fred K. Lamb  
University of Illinois at Urbana-Champaign  
Department of Physics  
1110 West Green Street  
Urbana, IL 61801

Prof. Charles A. Langston  
Geosciences Department  
403 Deike Building  
The Pennsylvania State University  
University Park, PA 16802

Jim Lawson, Chief Geophysicist  
Oklahoma Geological Survey  
Oklahoma Geophysical Observatory  
P.O. Box 8  
Leonard, OK 74043-0008

Prof. Thorne Lay  
Institute of Tectonics  
Earth Science Board  
University of California, Santa Cruz  
Santa Cruz, CA 95064

Dr. William Leith  
U.S. Geological Survey  
Mail Stop 928  
Reston, VA 22092

Mr. James F. Lewkowicz  
Phillips Laboratory/GPEH  
Hanscom AFB, MA 01731-5000( 2 copies)

Mr. Alfred Lieberman  
ACDA/VI-OA State Department Building  
Room 5726  
320-21st Street, NW  
Washington, DC 20451

Prof. L. Timothy Long  
School of Geophysical Sciences  
Georgia Institute of Technology  
Atlanta, GA 30332

Dr. Randolph Martin, III  
New England Research, Inc.  
76 Olcott Drive  
White River Junction, VT 05001

Dr. Robert Masse  
Denver Federal Building  
Box 25046, Mail Stop 900  
Denver, CO 80225

Dr. Gary McCartor  
Department of Physics  
Southern Methodist University  
Dallas, TX 75275

Prof. Thomas V. McEvilly  
Seismographic Station  
University of California  
Berkeley, CA 94720

Dr. Art McGarr  
U.S. Geological Survey  
Mail Stop 977  
U.S. Geological Survey  
Menlo Park, CA 94025

Dr. Keith L. McLaughlin  
S-CUBED  
A Division of Maxwell Laboratory  
P.O. Box 1620  
La Jolla, CA 92038-1620

Stephen Miller & Dr. Alexander Florence  
SRI International  
333 Ravenswood Avenue  
Box AF 116  
Menlo Park, CA 94025-3493

Prof. Bernard Minster  
IGPP, A-025  
Scripps Institute of Oceanography  
University of California, San Diego  
La Jolla, CA 92093

Prof. Brian J. Mitchell  
Department of Earth & Atmospheric Sciences  
St. Louis University  
St. Louis, MO 63156

Mr. Jack Murphy  
S-CUBED  
A Division of Maxwell Laboratory  
11800 Sunrise Valley Drive, Suite 1212  
Reston, VA 22091 (2 Copies)

Dr. Keith K. Nakanishi  
Lawrence Livermore National Laboratory  
L-025  
P.O. Box 808  
Livermore, CA 94550

Dr. Carl Newton  
Los Alamos National Laboratory  
P.O. Box 1663  
Mail Stop C335, Group ESS-3  
Los Alamos, NM 87545

Dr. Bao Nguyen  
HQ AFTAC/TTR  
Patrick AFB, FL 32925-6001

Prof. John A. Orcutt  
IGPP, A-025  
Scripps Institute of Oceanography  
University of California, San Diego  
La Jolla, CA 92093

Prof. Jeffrey Park  
Kline Geology Laboratory  
P.O. Box 6666  
New Haven, CT 06511-8130

Dr. Howard Patton  
Lawrence Livermore National Laboratory  
L-025  
P.O. Box 808  
Livermore, CA 94550

Dr. Frank Pilotte  
HQ AFTAC/TT  
Patrick AFB, FL 32925-6001

Dr. Jay J. Pulli  
Radix Systems, Inc.  
2 Taft Court, Suite 203  
Rockville, MD 20850

Dr. Robert Reinke  
ATTN: FCTVTD  
Field Command  
Defense Nuclear Agency  
Kirtland AFB, NM 87115

Prof. Paul G. Richards  
Lamont-Doherty Geological Observatory  
of Columbia University  
Palisades, NY 10964

Mr. Wilmer Rivers  
Teledyne Geotech  
314 Montgomery Street  
Alexandria, VA 22314

Dr. George Rothe  
HQ AFTAC/TTR  
Patrick AFB, FL 32925-6001

Dr. Alan S. Ryall, Jr.  
DARPA/NMRO  
3701 North Fairfax Drive  
Arlington, VA 22209-1714

Dr. Richard Sailor  
TASC, Inc.  
55 Walkers Brook Drive  
Reading, MA 01867

Prof. Charles G. Sammis  
Center for Earth Sciences  
University of Southern California  
University Park  
Los Angeles, CA 90089-0741

Prof. Christopher H. Scholz  
Lamont-Doherty Geological Observatory  
of Columbia University  
Palisades, CA 10964

Dr. Susan Schwartz  
Institute of Tectonics  
1156 High Street  
Santa Cruz, CA 95064

Secretary of the Air Force  
(SAFRD)  
Washington, DC 20330

Office of the Secretary of Defense  
DDR&E  
Washington, DC 20330

Thomas J. Sereno, Jr.  
Science Application Int'l Corp.  
10260 Campus Point Drive  
San Diego, CA 92121

Dr. Michael Shore  
Defense Nuclear Agency/SPSS  
6801 Telegraph Road  
Alexandria, VA 22310

Dr. Matthew Sibol  
Virginia Tech  
Seismological Observatory  
4044 Derring Hall  
Blacksburg, VA 24061-0420

Prof. David G. Simpson  
IRIS, Inc.  
1616 North Fort Myer Drive  
Suite 1440  
Arlington, VA 22209

Donald L. Springer  
Lawrence Livermore National Laboratory  
L-025  
P.O. Box 808  
Livermore, CA 94550

Dr. Jeffrey Stevens  
S-CUBED  
A Division of Maxwell Laboratory  
P.O. Box 1620  
La Jolla, CA 92038-1620

Lt. Col. Jim Stobie  
ATTN: AFOSR/NL  
Bolling AFB  
Washington, DC 20332-6448

Prof. Brian Stump  
Institute for the Study of Earth & Man  
Geophysical Laboratory  
Southern Methodist University  
Dallas, TX 75275

Prof. Jeremiah Sullivan  
University of Illinois at Urbana-Champaign  
Department of Physics  
1110 West Green Street  
Urbana, IL 61801

Prof. L. Sykes  
Lamont-Doherty Geological Observatory  
of Columbia University  
Palisades, NY 10964

Dr. David Taylor  
ENSCO, Inc.  
445 Pineda Court  
Melbourne, FL 32940

Dr. Steven R. Taylor  
Los Alamos National Laboratory  
P.O. Box 1663  
Mail Stop C335  
Los Alamos, NM 87545

Prof. Clifford Thurber  
University of Wisconsin-Madison  
Department of Geology & Geophysics  
1215 West Dayton Street  
Madison, WI 53706

Prof. M. Nafi Toksoz  
Earth Resources Lab  
Massachusetts Institute of Technology  
42 Carleton Street  
Cambridge, MA 02142



Dr. Larry Turnbull  
CIA OSWR/NEED  
Washington, DC 20505

DARPA/RMO/SECURITY OFFICE  
3701 North Fairfax Drive  
Arlington, VA 22203-1714

Dr. Gregory van der Vink  
IRIS, Inc.  
1616 North Fort Myer Drive  
Suite 1440  
Arlington, VA 22209

HQ DNA  
ATTN: Technical Library  
Washington, DC 20305

Dr. Karl Veith  
EG&G  
5211 Auth Road  
Suite 240  
Suitland, MD 20746

Defense Intelligence Agency  
Directorate for Scientific & Technical Intelligence  
ATTN: DTIB  
Washington, DC 20340-6158

Prof. Terry C. Wallace  
Department of Geosciences  
Building #77  
University of Arizona  
Tucson, AZ 85721

Defense Technical Information Center  
Cameron Station  
Alexandria, VA 22314 (2 Copies)

Dr. Thomas Weaver  
Los Alamos National Laboratory  
P.O. Box 1663  
Mail Stop C335  
Los Alamos, NM 87545

TACTEC  
Battelle Memorial Institute  
505 King Avenue  
Columbus, OH 43201 (Final Report)

Dr. William Wortman  
Mission Research Corporation  
8560 Cinderbed Road  
Suite 700  
Newington, VA 22122

Phillips Laboratory  
ATTN: XPG  
Hanscom AFB, MA 01731-5000

Prof. Francis T. Wu  
Department of Geological Sciences  
State University of New York  
at Binghamton  
Vestal, NY 13901

Phillips Laboratory  
ATTN: GPE  
Hanscom AFB, MA 01731-5000

AFTAC/CA  
(STINFO)  
Patrick AFB, FL 32925-6001

Phillips Laboratory  
ATTN: TSML  
Hanscom AFB, MA 01731-5000

DARPA/PM  
3701 North Fairfax Drive  
Arlington, VA 22203-1714

Phillips Laboratory  
ATTN: SUL  
Kirtland, NM 87117 (2 copies)

DARPA/RMO/RETRIEVAL  
3701 North Fairfax Drive  
Arlington, VA 22203-1714

Dr. Michel Bouchon  
I.R.I.G.M.-B.P. 68  
38402 St. Martin D'Heres  
Cedex, FRANCE

Dr. Michel Campillo  
Observatoire de Grenoble  
I.R.I.G.M.-B.P. 53  
38041 Grenoble, FRANCE

Dr. Jorg Schlittenhardt  
Federal Institute for Geosciences & Nat'l Res.  
Postfach 510153  
D-3000 Hannover 51, GERMANY

Dr. Kin Yip Chun  
Geophysics Division  
Physics Department  
University of Toronto  
Ontario, CANADA

Dr. Johannes Schweitzer  
Institute of Geophysics  
Ruhr University/Bochum  
P.O. Box 1102148  
4360 Bochum 1, GERMANY

Prof. Hans-Peter Harjes  
Institute for Geophysics  
Ruhr University/Bochum  
P.O. Box 102148  
4630 Bochum 1, GERMANY

Prof. Eystein Husebye  
NTNI/NORSAR  
P.O. Box 51  
N-2007 Kjeller, NORWAY

David Jepsen  
Acting Head, Nuclear Monitoring Section  
Bureau of Mineral Resources  
Geology and Geophysics  
G.P.O. Box 378, Canberra, AUSTRALIA

Ms. Eva Johannisson  
Senior Research Officer  
National Defense Research Inst.  
P.O. Box 27322  
S-102 54 Stockholm, SWEDEN

Dr. Peter Marshall  
Procurement Executive  
Ministry of Defense  
Blacknest, Brimpton  
Reading FG7-FRS, UNITED KINGDOM

Dr. Bernard Massinon, Dr. Pierre Mechler  
Societe Radiomana  
27 rue Claude Bernard  
75005 Paris, FRANCE (2 Copies)

Dr. Svein Mykkeltveit  
NTNT/NORSAR  
P.O. Box 51  
N-2007 Kjeller, NORWAY (3 Copies)

Prof. Keith Priestley  
University of Cambridge  
Bullard Labs, Dept. of Earth Sciences  
Madingley Rise, Madingley Road  
Cambridge CB3 0EZ, ENGLAND